

# PUBLISHED VERSION

Iain Murray Reid

**MF and HF radar techniques for investigating the dynamics and structure of the 50 to 110 km height region: a review**

Progress in Earth and Planetary Science, 2015; 2(1):33-1-33-34


© 2015 Reid. Open Access This article is distributed under the terms of the Creative Commons Attribution 4.0 International License (<http://creativecommons.org/licenses/by/4.0/>), which permits unrestricted use, distribution, and reproduction in any medium, provided you give appropriate credit to the original author(s) and the source, provide a link to the Creative Commons license, and indicate if changes were made.

Originally published at:

<http://doi.org/10.1186/s40645-015-0060-7>

## PERMISSIONS

<http://creativecommons.org/licenses/by/4.0/>



**Attribution 4.0 International (CC BY 4.0)**

This is a human-readable summary of (and not a substitute for) the [license](#). [Disclaimer](#).


**You are free to:**

- Share** — copy and redistribute the material in any medium or format
- Adapt** — remix, transform, and build upon the material for any purpose, even commercially.

The licensor cannot revoke these freedoms as long as you follow the [license terms](#).

**Under the following terms:**

- Attribution** — You must give [appropriate credit](#), provide a link to the license, and [indicate if changes were made](#). You may do so in any reasonable manner, but not in any way that suggests the licensor endorses you or your use.
- No additional restrictions** — You may not apply legal terms or [technological measures](#) that legally restrict others from doing anything the license permits.



10 August 2017

<http://hdl.handle.net/2440/106608>

REVIEW

Open Access



# MF and HF radar techniques for investigating the dynamics and structure of the 50 to 110 km height region: a review

Iain Murray Reid<sup>1,2</sup> 

## Abstract

The application of medium-frequency (MF) and high-frequency (HF) partial reflection radar to investigate the neutral upper atmosphere is one of the oldest such techniques still regularly in use. The techniques have been continuously improved and remain a robust and reliable method of obtaining wind velocities, turbulence intensities, electron densities, and measurements of atmospheric structure in the mesosphere lower thermosphere (MLT) region (50 to 110 km). In this paper, we review recent developments, discuss the strengths and weaknesses of the technique, and consider possible improvements.

**Keywords:** Medium-frequency radar techniques; High-frequency radar techniques; Partial reflection radar; Spaced antenna technique; Full correlation analysis; Mesosphere lower thermosphere region; D region; MLT region dynamics; Meteor radar; Imaging Doppler interferometer

## Review

### Introduction

This review is about the investigation of the upper neutral atmosphere in the 50 to 110 km height region by radars operating in the medium-frequency (MF, 0.3–3 MHz) and high-frequency (HF, 3–30 MHz) bands. In the MF band, the focus is on the range from about 2 to 3 MHz and in the HF band on the frequency range up to around 3.2 MHz. These radars are sometimes referred to as partial reflection (PR) radars and make use of the ionized component of the atmosphere as a tracer for the neutral motions in the ionosphere between heights of around 50 to 110 km. We do not consider the case of total reflection from the ionosphere, except where it complicates partial reflection radar measurements of the neutral atmosphere. Of course, we do consider other results where appropriate.

The 50 to 110 km height range is generally referred to as the mesosphere and lower thermosphere (MLT). The mesosphere is that region between the temperature maximum near 50 km (the stratopause) and the temperature minimum near 85 km (the mesopause). The

thermosphere lies above the mesosphere. It is perhaps worth noting that the actual boundary heights change with location and season, and the mesopause height may be nearer 100 km at mid-latitudes in winter (e.g., Fan et al. 2014).

The state of the MLT is determined by dynamical coupling from below via waves and by photoionization from above by the sun. The basic thermal structure is set by the balance between absorption of solar UV and infrared radiation to space, but it is significantly modified by momentum deposition by atmospheric waves, notably internal atmospheric gravity (buoyancy) waves, that drives the atmosphere away from radiative equilibrium. For example, this causes the summer polar MLT to be up to 100 K colder than radiative equilibrium acting alone and the winter polar MLT to be correspondingly warmer (e.g., Andrews et al. 1987).

The investigation of the MLT region relies largely on remote sensing techniques. The direct techniques available generally rely on rocket delivered instruments, and so observations are necessarily episodic in nature. Indirect techniques include passive (airglow) and active (lidar) optical and radar techniques. A form of radar, the focus of this paper, was used to confirm the existence of the ionosphere (Appleton and Barnett 1925; Breit and Tuve 1925,

Correspondence: iain.reid@adelaide.edu.au

<sup>1</sup>Department of Physics, School of Physical Sciences, The University of Adelaide, Adelaide 5005, Australia

<sup>2</sup>ATRAD Pty Ltd, 20 Phillips Street, Thebarton 5031, Australia

1926), and radar has since been extensively used to investigate its properties.

There are two main mechanisms believed to result in coherent returns of radio waves from the MLT region. These are turbulent (or Bragg) scatter and Fresnel Reflection or Fresnel Scatter. Bragg scatter results from radar returns from turbulent irregularities in the electron density with scales of half the projection of the radar wavelength onto the wave vector. Fresnel reflection (also known as partial reflection) results from the presence of irregularities in refractive index transverse to the beam direction which are thin compared to the radar wavelength. Fresnel scatter results when the scattering medium is coherent in the two dimensions transverse to the probing wave and random in the direction parallel to the wave vector. This might correspond to a sharply bounded region of turbulence, for example. Generally at the MF/HF frequencies that we are considering here, the radar returns are produced by Fresnel reflection or Fresnel scatter. However, it is noteworthy in this context that the detailed nature of the backscattering and partially reflecting irregularities in the MLT is still not well understood.

The MLT height region corresponds to the ionospheric D region and the lower part of the ionospheric E region. The E region extends from heights of about 90 to 140 km and reaches its peak ionization levels near 110 km near noon. The actual peak height and height extent of the E region is dynamic, and it varies with location, time of day, season, solar cycle, and solar activity. The D region is that part of the ionosphere lying below the E region, and its lowest extent is about 50 km. Again, this lower bound is dynamic and depends strongly on location, time of day, and solar activity. Likewise, its upper extent is dynamic, and it varies with the changes in the extent of the E region. During the day, ionization rates in the D region are determined by solar Lyman- $\alpha$  (Ly- $\alpha$ ; ~65–80 km), solar X-rays ( $\geq 80$  km) and galactic cosmic ray fluxes ( $\leq 65$  km), and at night by solar Ly- $\alpha$  and Lyman- $\beta$  (Ly- $\beta$ ) scattered from the geocorona (~80–90 km) and by galactic cosmic ray fluxes (e.g., Nicolet and Aikin 1960; Thomson et al. 2007; Hedin et al. 2008; Pavlov 2014).

It is sometimes suggested that the D region can be considered to be formed by two different “layers”: a “D layer” formed by the solar photoionization of NO by Ly- $\alpha$  and peaking near 90 km, and a “C layer” near 64 to 68 km formed by cosmic ray ionization (e.g., Deeks 1966; Bain and May 1967; Abdu et al. 1973). The idea of the C layer was first introduced to understand very low frequency (VLF, 3–30 kHz) radar propagation observations. In more recent work, Bertoni et al. (2013) briefly review some of these and suggest that a C layer of enhanced electron density does exist near 64 to 68 km for a few hours after dawn, but that its formation is associated with sunrise

rather than with cosmic ray ionization. However, in the 50 to 110 km height region, the concept of a clear division between “E” and “D” regions and single “D” and “C” layers is slightly misleading, as the 50 to 100 km height region is stratified (e.g., Reid 1990), and most often consists of multiple regions of enhanced backscatter, with a tendency for this to occur at certain “preferred” heights for radar returns (e.g., Gregory 1961; Titheridge 1962; Reid 1990). This strong tendency to form layer-like regions of enhanced backscatter is overlaid with a strong diurnal variation in the heights of occurrence of radar returns. Near 85–90 km, a layer persists both day and night, and during the day, partial reflections extend down to heights near 50 km. This behavior might be a more logical justification for splitting the D region into D and C layers.

Whatever the actual height extent of the D region, or its subdivisions, in this review, we are focused on partial reflection of radar returns from the ionosphere in the region above 50 km, and below the total reflection height of the E region, for the purposes of investigating the neutral atmosphere.

#### *Brief historical overview*

##### **Partial reflection from the 50 to 100 km height region**

Echoes that appeared to be from mesospheric heights were reported as early as 1930 (Appleton 1930), and in the years that followed, a number of reports of echoes, mainly not only from the 50–100 km height interval but also some of uncertain origin from the 15 to 65 km height range (see e.g., Watson-Watt et al. 1937) were made. These early observations were all obtained from low frequencies (LF, 30–300 kHz) to HF and are summarized in Ellyett (1947) and Ellyett and Watts (1959). The first unequivocal indications of radar that returns from heights near but below the E region appear to be those presented by Appleton and Piddington (1938). They found echoes below the E region (~110 km) and which extended down to heights of about 80 km. Their results were obtained at MF using an ionosonde and were followed by similar results at MF and HF obtained by Dieminger (1952), Dieminger and Hofmann-Heyden (1952), and by Gnanalingham and Weekes (1952).

The work of Dieminger represents the first systematic investigation of the characteristics of these echoes and is not inconsistent with present knowledge. The first results of an experiment specifically designed to investigate the lower ionosphere below the E region were presented by Gardner and Pawsey (1953). The ordinary (O) and extraordinary (E or X) magnetoionic components each suffer different amplitude and phase variations with height due to the height variations in electron density ( $N_e$ ) and collision frequency ( $\nu$ ) (e.g., Thrane and Piggott 1966; Friedrich and Torkar 1983; Holdsworth

et al. 2002; Vuthaluru et al. 2002), and this was exploited by Gardner and Pawsey to measure the electron densities. The technique they used was the foundation of the differential absorption experiment (DAE) and differential phase experiment (DPE), amongst the few techniques capable of providing regular ground-based measurements of electron density in the mesosphere (for reviews, see Belrose 1970; Manson and Meek 1984). They also found that the ionization had a tendency to form in strata near 70 and 90 km.

As we have noted above, the evidence that there is a tendency for layers observed by radar to occur at certain preferred heights regardless of location has a long history. For example, Dieminger (1952), Gregory (1956, 1961), Titheridge (1962), Reid (1990), Jones et al. (2004), and Hall et al. (2006) discuss this for MF and HF, Bailey et al. (1955) and Pineo (1956) for very high frequency (VHF; 30 to 300 MHz) forward scatter results, Bowles et al. (1964) for both vertical and forward scatter VHF results, and Flock and Balsley (1967) for vertical incidence VHF results. At MF/HF, such preferred heights are subject to seasonal and annual variations, but persistent echoes occur from mean heights of about 65–68, 74–75, 83–85, and 92 km. The origin of the layers below 80 km is not well understood and could be aeronomic, dynamical, or a combination of both in origin. Layers do appear near sunrise and disappear near sunset, and so photo detachment is suggested.

The authors noted above, and many others, have found that one of the most persistent regions of echo occurrence is that near 70–75 km. This particular preferred height seems to be related to an equally persistent temperature inversion in the same height range (Schmidlin 1976; Champion 1987; Offermann et al. 1987; Hauchecorne et al. 1987), and Hauchecorne et al. (1987) suggest a similar height variation in the inversion to that found in VHF echo occurrence and that an enhancement in gravity wave breaking occurs in the region of increased stability in and above the temperature minimum. This idea has not been explored in a systematic manner using a modern MF/HF radar collocated with other observing instruments, the ideal instrument being a LIDAR. This, and the underlying formation mechanisms for the other preferred heights, is a topic certainly worth for future investigation.

#### ***Investigation of dynamics in the 50 to 100 km height region***

In the MLT region, the first attempts to measure the motion of the ionosphere used spaced receiving antennas to measure the apparent motion of the ground diffraction pattern across the observing region (e.g., Ratcliffe and Pawsey 1933; Mitra 1949; Krautkrämer 1950). These early results were for total reflections from the ionosphere, and spaced antenna (SA) measurements ultimately proved very difficult to interpret when applied to total reflection

from the ionosphere if the object was to measure neutral atmospheric dynamics, and they are not suitable for this purpose. Spaced antenna techniques are still used for investigating ionospheric dynamics in the form of ionosondes and dynasondes, and Reinisch et al. (1998) and Rietveld et al. (2008) give contemporary accounts of this application.

Gardner and Pawsey's (1953) work laid the foundations for an entire field of study for measuring electron densities and investigating the structure of the D region MLT region, and weak D region partial reflections and backscatter were subsequently exploited using a SA technique to investigate the dynamics of the neutral atmosphere (Fraser 1965). Both Gardner and Pawsey's and Fraser's techniques are still in use in essentially the same basic experimental form as they were more than 60 and 50 years ago, respectively.

The evolution of MF/HF SA techniques since the 1950s has followed the development of radar hardware and computing. In 1965, Fraser (1965) used the spaced antenna technique to determine partial reflection winds at Birdling's Flat near Christchurch in New Zealand using a simple binary correlation analysis. A more complete description is included in Fraser (1965). Stubbs (1973) used the Buckland Park medium frequency (BPMF) array to make SA measurements and analyzed them using the full correlation analysis (FCA) to determine D region winds. The FCA is a more sophisticated correlation analysis for the SA experiment which we will discuss below. Stubbs also validated the MF SA FCA winds against meteor radar winds from a nearby location.

Originally, data analysis generally took place offline and offsite, and most observing sites were limited to operation on a campaign basis. The advent of cheap personal computers allowed the introduction of the first real-time analysis of the SA experiment with a simplified FCA, the so-called poor man's FCA (Meek 1980). The original system hardware used in the SA experiment often only measured the amplitude of the returned radio waves, and phase information was not generally available. An example of the amplitude-only variation of radio waves received at one antenna on the BPMF radar in the 1970s is shown in Additional file 1: Video 1. This variation in amplitude was originally referred to as "fading", and the mean fading time is still one of the output parameters of a typical SA analysis (see Table 5).

Later, once coherent receiver systems were introduced, phase information became available, and Doppler-based and interferometric techniques became more common at MF (e.g., Vincent and Reid 1983; Adams et al. 1986). The most sophisticated ultimate implementation of this was perhaps the development of the BPMF radar (Reid et al. 1995) which included 30 independent phase-controlled transmitters and 16 independent receivers,

allowing great flexibility in experimental configurations (e.g., Holdsworth and Reid 2004a). Currently, the Saura HF large array radar is the most capable in the world (Singer et al. 2008).

In the sections below, we explore the application of MF/HF radar techniques to investigate the MLT region, consider their weaknesses and strengths, and suggest possible future developments.

#### **MF and HF radar techniques for the MLT region**

There are a variety of radar techniques available for investigating the MLT region. These split naturally into those that use the ionization produced by solar radiation as a target and those that use ionized trails produced by meteors as targets. A number of these techniques are summarized in Table 1. Each technique has its own strengths and weaknesses, and it has become more common to utilize clusters of instruments to investigate the MLT region in order to maximize strengths and minimize weaknesses. For completeness, we have included two techniques in this table that are no longer used. These are the LF ionospheric drift experiment (see Sprenger and Schminder 1969; Jacobi 2014) which used transmitters of opportunity, in the form of commercial broadcast radio transmitters, and the “partial reflection experiment” (PRE) radar for measuring electron densities which was established near Tromsø, Norway in 1975 (see Brekke et al. 1985). This radar was the last of the large dedicated instruments for measuring electron densities in the lower ionosphere (see Belrose 1970 for a summary of instruments existing at that time). The Tromsø radar now operates in modified form as an MF SA FCA radar (e.g., Hall 2000). As we note briefly below, the ability to measure electron densities has been incorporated into newer MF/HF SA and Doppler beam swing (DBS) radars (see e.g.,

Holdsworth et al. 2002; Holdsworth and Reid 2004a; Singer et al. 2011).

In the last decade, this reapplication of older techniques and the validation of existing techniques for measuring neutral winds in the MLT region have emerged. In addition to measuring electron densities, these include the use of dynasondes for measuring neutral winds in the MLT (Jones et al. 2003) and the use of super dual auroral radar network (SuperDARN) ionospheric radars as meteor radars (e.g., Kleinknecht et al. 2014).

While the application of radars operating in the MF and HF bands to investigate the neutral upper atmosphere is one of the oldest such techniques still regularly in use, the techniques have been continuously improved, largely through the availability of better hardware (e.g., Reid et al. 1995; Holdsworth and Reid 2004b; Singer et al. 2008; Li et al. 2012) and readily available and economical but powerful computers, and provide a robust and reliable method of obtaining wind velocities (e.g., Stubbs 1973; Pancheva et al. 2002), turbulence intensities (e.g., Hocking 1983; Holdsworth et al. 2001), electron densities and collision frequencies (e.g., Thrane and Piggott 1966; von Biel 1977; Friedrich and Torkar 1983; Holdsworth et al. 2002; Singer et al. 2011), measurements of atmospheric structure (e.g., Gregory 1956; Hall 2000), temperatures (e.g., Tsutsumi et al. 1999; Holdsworth et al. 2006), and measurements of energy and momentum transfer (e.g., Reid and Vincent 1987; Murphy and Vincent 1993; Placke et al. 2015) in the MLT region.

There have been a number of reviews of the techniques. Briggs (1980) carefully describes the underlying principles of SA and DBS measurements of the neutral atmosphere, and Whitehead et al. (1983) provides a complementary review, which extends the discussion to ionospheric measurements. Briggs (1992, 1994) provides

**Table 1** Radar techniques for investigating the MLT region

Radar technique	Typical frequency (wavelength)	Frequency range	Typical height coverage	Height resolution	Time resolution	Measured quantities	Status
Meteor radar	30 MHz (10 m)	MF to UHF	75–110 km	1–5 km	30–60 min	$u, v, T, \rho$ , radiants, meteoroid velocities	Current
LF ionospheric spaced antenna drift	200 kHz (1500 m)	200 kHz (1500 m)	90–100 km (night)	1 height uncertainty ~2 km	1 min	$u, v$	Retired
Dedicated DAE/DPE PR radar	3 MHz (100 m)	3 MHz (100 m)	60–90 km (day) 85–100 km (night)	1–3 km	1–5 min	$N_e, u$	Retired
MF/HF PR SA radar	3 MHz (100 m)	1.94 to 3.18 MHz	60–100 km (day) 80–100 km (night)	1–3 km	1–5 min	$u, v, N_e, u$	Current
MST radar	50 MHz (6 m)	44.75 to 64 MHz	0.5–20 km 60–80 km (day)	150–600 m	5 min	$u, v, w$	Current
SuperDARN radar	12 MHz (25 m)	8–20 MHz	As for meteor radar	As for meteor radar	As for meteor radar	As for meteor radar	Current

The symbols represent the following parameters:  $u$  is the zonal wind magnitude,  $v$  is the meridional wind magnitude,  $w$  is the vertical wind magnitude,  $T$  is the temperature,  $\rho$  is the neutral density,  $N_e$  the electron number density, and  $u$  is the collision frequency



a general overview and history of MF/HF radar techniques of direct relevance to this review that can be applied to the MLT region. Reid (1996) reviewed MF techniques in terms of their ability to make measurements of mean winds, atmospheric tides, and gravity waves, and Hocking (1997) considers the strengths and limitations of mesosphere stratosphere troposphere (MST) radar measurements of middle atmosphere winds with a focus directly related to MF and HF radar techniques. Reid et al. (1995) and Holdsworth and Reid (2004a, 2004b) provide an overview of the capabilities of the BPMF radar which serves as a good description of the capabilities of MF/HF radars generally, Holdsworth et al. (2004a) provide a good description of a modern all-sky meteor radar, Fraser (2005) provides a history of the development of scientific radar in New Zealand very relevant to this review, and Hocking (2011) provides a general review of radar techniques for investigating the MLT region.

As we noted above, in this review, we concentrate on MF/HF SA radar techniques for measuring the neutral atmosphere using returns from the ionized atmosphere, but include meteor radars where relevant. The most common meteor radar operating frequencies are currently in the lower VHF band, between 30 and 55 MHz, but there are advantages to operating at lower frequencies because the meteor count rate  $N$  goes as (McKinley 1951)

$$N \propto \frac{P_T^{1/2} G \lambda^{3/2}}{P_R^{1/2}}$$

where  $\lambda$  is the radar wavelength,  $P_T$  is the transmitted power,  $G$  is the system gain, and  $P_R$  is the received power. Meteor radars historically operated close to, and often below, 30 MHz. The peak of the meteor detection distribution is also higher with a lower frequency (e.g., Younger et al. 2014). This makes SuperDARN radars (8 to 20 MHz) potentially very powerful meteor radars for measuring winds at heights in the data poor region between above 100 and 120 km.

MF radars have been successfully used as meteor radars, particularly, but not exclusively, at higher latitudes (e.g., Tsutsumi et al. 1999; Holdsworth and Reid 2004a; Tsutsumi and Aso 2005), and for measuring winds up to 120 km. However, a disadvantage here is that as the frequency is lowered, meteor detections are harder to discriminate from ionospheric echoes. In addition, above about 110 km, the Earth's magnetic field increasingly influences the motion of the ionized component of the atmosphere, (e.g., Elford and Elford 2001), and so both the SA and meteor techniques may not measure the neutral dynamics above this height.

The radar techniques applied at MF and at HF to investigate the MLT height region are basically the same techniques that can be applied at other radar frequencies.

They differ in that the wavelengths in the MF and HF bands are relatively long (1000 to 100 m in the MF band; 100 to 10 m in the HF band), in that ionospheric radar returns are generally present above 80 km both day and night at these frequencies as we shall see below, and in that the irregularities responsible for the backscatter and partial reflection are very aspect sensitive at these frequencies (see e.g., Pawsey 1935; Holdsworth and Reid 2004a). These differences give rise to a number of unique considerations which we discuss below.

### **Spaced antenna techniques**

The most common technique applied at MF and lower HF is the SA technique, and MF/HF radars currently operating using the technique are summarized in Table 2 along with some of their operating characteristics. Radars of this type that have been retired since the review of Reid (1996) are summarized in the same way in Table 3. Some of these radars were only ever intended to provide shorter term observations, but for others, ongoing long-term funding has proved difficult to obtain. Figure 1 shows the location of the radars summarized in Tables 2 and 3.

In SA techniques, a minimum of three non-collinear receiving antennas are used to receive partial reflections from the D region. The transmitting antenna used is usually located very close to the receiving antennas in a bi-static configuration. More commonly, the same antennas are used for both transmission and reception. A typical antenna arrangement is shown in Fig. 2. In this particular case, which is for the Poker Flat MF radar (see e.g., Kawamura et al. 2007), all four antennas are used for both transmission and reception, and each antenna is connected to an independent receiver. Another arrangement is shown in Fig. 3, which is for the Saura HF radar (Singer et al. 2011). The long arms allow this radar to be used in DBS mode, and the antennas shown in green allow it to be used as a SA radar. In DBS, narrow beams are formed in order to measure the radial velocities in three or more beam directions, and the horizontal and vertical winds are calculated from the radial velocities.

The D region ionosphere is birefringent, and both ordinary (O) and extraordinary (E or X) polarizations are used. The E mode is strongly absorbed during the day, so historically, for wind measuring radars, the E mode was used at night and the O mode during the day. For this reason, the antennas shown in Fig. 2 are crossed dipoles. This allows both modes to be transmitted and received. It is now common to transmit O and E modes on either alternate radar pulses, or on alternate data records, and then apply the DAE or DPE to measure the electron density (see e.g., Holdsworth et al. 2002; Singer et al. 2003; Singer et al. 2011).

**Table 2** A summary of current MF/HF SA radars

Facility	Lat/long	Mode	Freq. (MHz)	Power (kW)
Adelaide, Australia	35 S, 138 E	SA, IDI, DBS	1.98	100
Andenes, Norway	69 N, 16 E	SA	1.98	50
Bear Lake, USA	42 N, 111 W	IDI	2.2 (day), 3.8 (night)	10
Christchurch, NZ	44 S, 172 E	SA	2.40	100
Davis Station, Antarctica	69 S, 78 E	SA	1.98	25
Kolhapur, India	16.8 N, 74.2 E	SA	1.94	25
Juliusruh, Germany	55 N, 13 E	SA, IDI, DBS	3.18	128
Langfang, China	39.41 N, 116.71 E	SA	1.99	64
Pameungpeuk, Indonesia	7.7 S, 107.7 E	SA	2.008	30
Poker Flat, USA	65 N, 148 W	SA	2.43	50
Pontianak, Indonesia	0 S, 109 E	SA	1.98	25
Qijing, China	25.6 N, 103.8 E	SA	2.138	64
Saskatoon, Canada	52 N, 107 W	SA	2.22	50
Saura, Norway	69 N, 16 E	SA, IDI, DBS	3.17	116
Scott Base, Antarctica	78 S, 167 E	SA	2.90	60
Syowa Base, Antarctica	69 S, 39.6 E	SA	2.4	50
Tirunelveli, India	8.7 N, 77.8 E	SA	1.98	25
Tromso, Norway	70 N, 19 E	SA	2.78	50
Wakkanai, Japan	45.4 N, 141.7 E	SA	1.955	50

The radar at Bear Lake is a dynasondes that can operate in an IDI mode. The most recent MF radar installations have been in China, as part of the Chinese Meridian project. The Indian radars and the Saura 3.18 MHz radar (IAP, Germany) have been recently upgraded

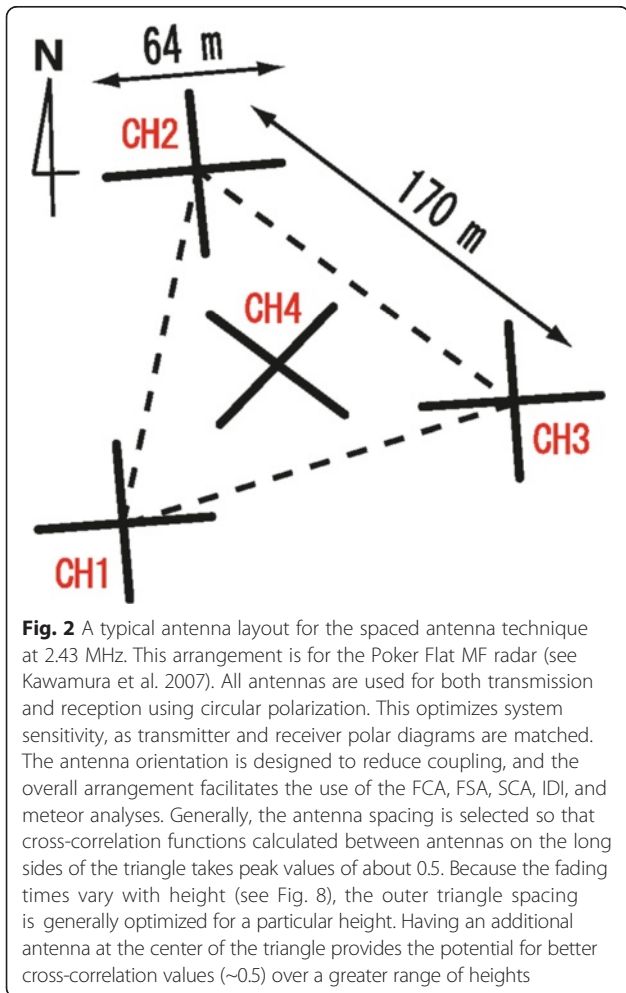
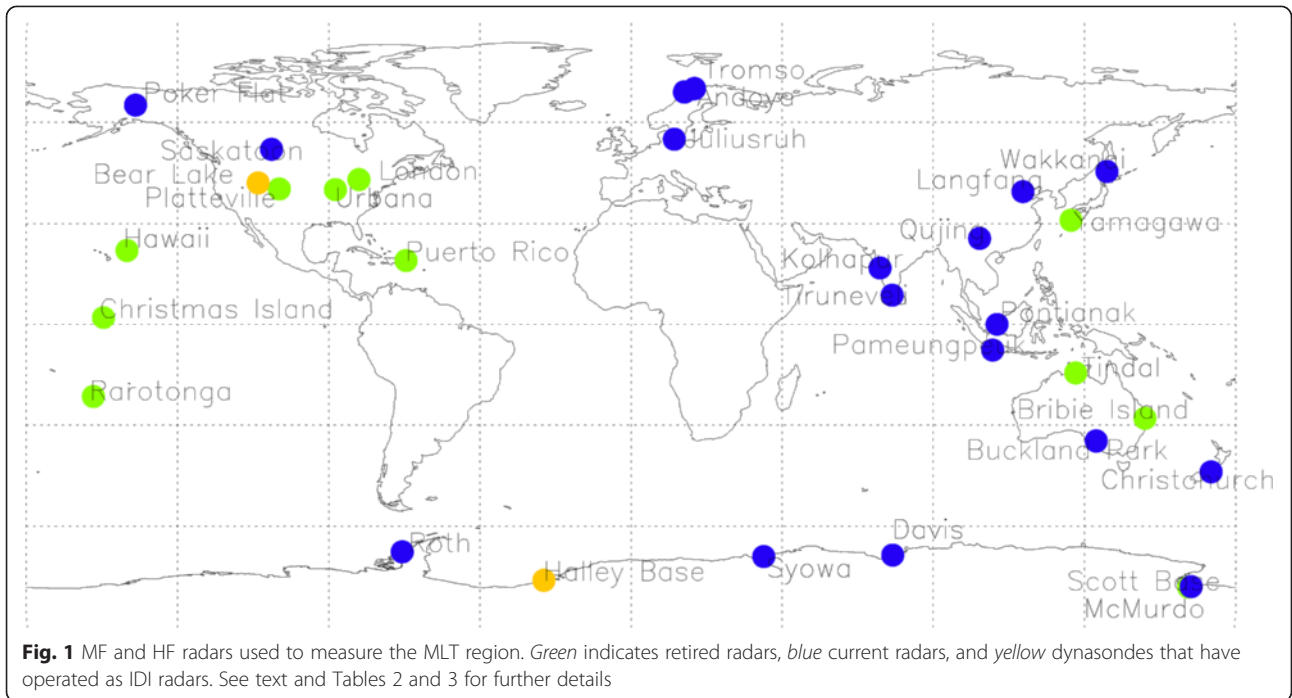
Figure 4 shows one example from Singer et al. (2003) which shows the electron densities derived from the DAE and DPE, as well as the O and X mode signal powers obtained using interleaved operation.

Vertical incidence pulsed transmission is used for all current MF/HF SA systems. A unique frequency modulated continuous wave chirp (FMCW-chirp) 3.18 MHz system was operated at Juliusruh in Germany for a number of years. This system commenced operation in 1982

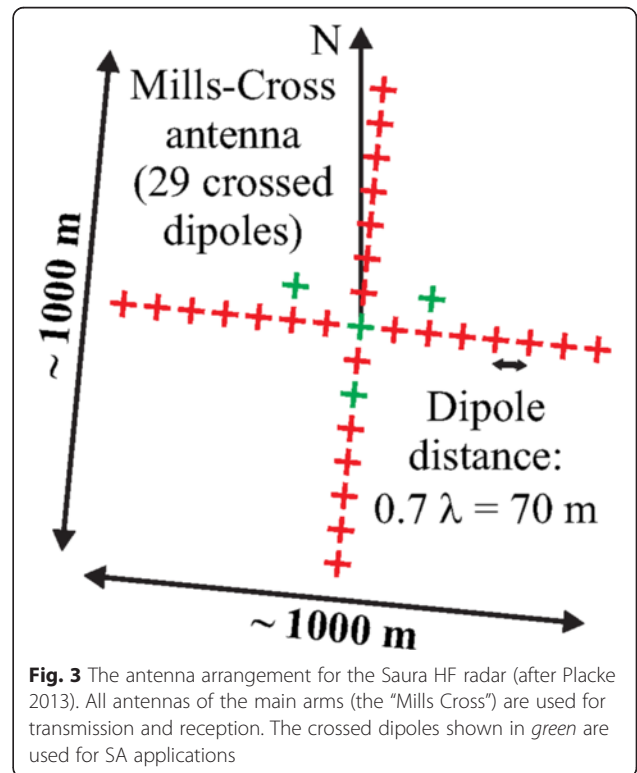
**Table 3** MF/HF radars that have been retired since the review of Reid (1996)

Facility	Lat/long	Mode	Freq. (MHz)	Power (kW)	Remarks
Bribie Island, Australia	28 S, 153 E	SA, DBS	1.98	25	Long term
Christmas Island	2 N, 157 W	SA	1.98	25	Long term
Halley Base, Antarctica	76S, 26 W	IDI	2.75	10	Long term
Hawaii, USA	22 N, 156 W	SA	1.98	25	Long term
London, Canada	43 N, 81 W	SA	2.22	25	Long term
McMurdo, Antarctica	78 S, 166 E	SA	1.98	50	Long term
Nanjing, China	32 N, 119 E	SA	2.00	25	Long term
Platteville, USA	40 N, 105 W	SA	2.219	25	Long term
Puerto Rico	19 N, 67 W	SA	1.95	25	Long term
Rarotonga, Cook Islands	22 S, 160 W	SA	1.98	25	Long term
Robsart, Canada	49 N, 109 W	SA	2.22	25	Campaign
Sylvan Lake, Canada	52 N, 114 W	SA	2.22	25	Campaign
Tindal, Australia	15 S, 132 E	SA	1.98	25	Campaign
Urbana, USA	40 N, 88 W	SA	2.66	25	Long term
Yamagawa, Japan	31 N, 131 E	SA	1.95	50	Long term

The Halley dynasonde operated successfully in IDI mode until it was relocated in 2008



to measure electron densities (Priese and Singer 1984; Singer et al. 1988) and was modified to be capable of making spaced antenna measurements in 1990 (e.g., Hoffmann et al. 1990). It was replaced with a pulsed system in 2005 (e.g., Hoffmann et al. 2011).





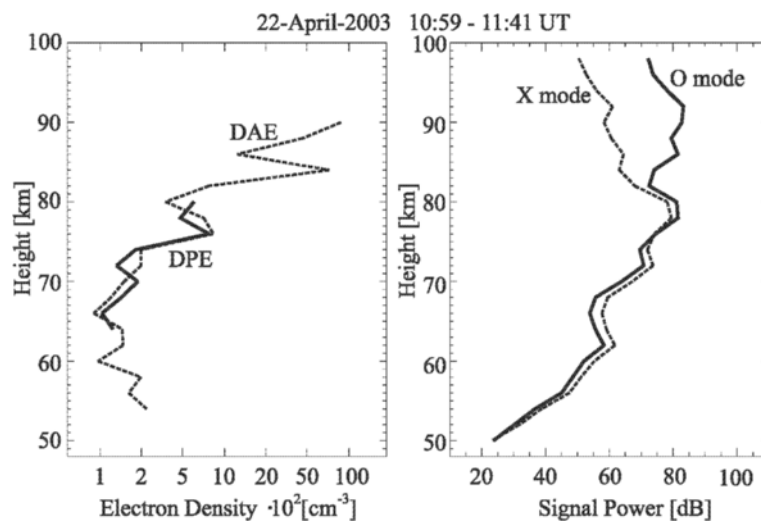


**Fig. 4** Electron densities derived from the DAE and DPE using the Saura HF radar (left panel) and the corresponding signal powers for the ordinary (O mode) and X modes obtained using interleaved observations (right panel) (after Singer et al. 2003)

With a typical 3 dB pulse width of 26.6  $\mu\text{s}$  for a system operating at 2 MHz, the height resolution is about 4 km, which is commonly oversampled to yield a 2 km range bin. However, as we discuss below, because of the presence of the strong returns from the E region, it would be preferable to use a shorter pulse. At 2 MHz, the wavelength is 150 m, so a 4 km resolution at 2 MHz is comparable to a 160 m height resolution for a 50 MHz (6 m wavelength) atmospheric radar. A more typical best range resolution at 50 MHz would be 100 m, which would correspond to a 2.5 km pulse width at 2 MHz. A 1 km pulse width (which would be 1.6 km at 2 MHz) is used successfully on the 3.17 MHz Saura radar (e.g., Singer et al. 2008, 2011).

The maximum usable pulse repetition frequency (PRF) is determined by the total reflection height. An illustrative range time diagram is shown in Fig. 5. This is taken

from Czechowsky et al. (1983) and shows two pulse repetition periods (PRP =  $\tau$ ), of 1 and 4 ms, corresponding to PRFs of 1000 and 250 Hz, respectively. In simple range aliased terms, the maximum unaliased range  $r_{\text{max}}$  is given by

$$r_{\text{max}} = c\tau/2,$$

where  $c$  is the speed of light, and so these PRFs would correspond to maximum usable ranges of 150 and 600 km, respectively. However, as the figure shows, returns from ranges 1, 2, and 3 in the E region appear at lower ranges at later times as a consequence of multiple reflections from the E region. At E region heights, and at MF and lower HF during the day, these returns would most likely be from total reflections. Consequently, we

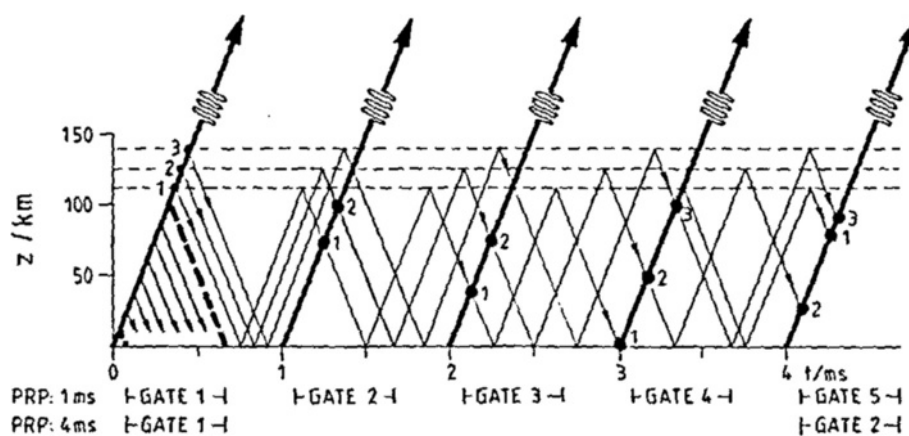


**Fig. 5** Range-time diagram showing the influence of multiple reflections or scattering at E region heights on the received signals for two different pulse repetition periods (after Czechowsky et al. 1983). For the case of total reflection from the E region, the returns would be attenuated by each ground reflection and by any absorption through the D region. This is significant during daytime

expect these returns to be very strong and to potentially dominate the weaker partial reflections (typically  $10^{-3}$  to  $10^{-5}$  that of the E region) from the D region. Of course, the strength of these returns would be reduced by each ground reflection and by any D region absorption present during each transit, but the returns could still be strong enough to contaminate the weak D region returns even after multiple reflections. D region absorption is very strong during the day. As a consequence of this, with typical E region peak heights during the day of 110 km, and typical F region peak heights of above 210 km during the night, PRF values from 80 to 120 Hz during the day and from 20 to 40 Hz at night are used.

These restrictions on PRF mean that the duty cycles of PR radars are low, and in this, the radars could be considered to be underutilized. The use of pseudo-random pulse codes and of pulse stuttering on transmission are avenues for investigation that could lead to better use of such radar's capabilities.

#### **Choice of operating frequency**

Most MF/HF SA radar techniques for investigating the neutral atmosphere do not routinely make measurements above about 100 km. This is because a significant issue with radars operating at less than the critical frequency for the E region (between 2 and 4 MHz depending on latitude, time of day, season, and solar cycle; see e.g., Jursa et al. 1985) is that the total reflection height varies between around 95 and 110 km. This represents an upper operating height during the day for radars operating in the MF and lower HF bands. In addition, close to, but below the total reflection height, group retardation means the reported heights (the virtual heights) are greater than the actual backscatter/partial reflection heights. This results in different ranges (that is, group delays) corresponding to very similar heights. This also means that the maximum useable height is not fixed for a particular frequency radar or location, and the actual maximum useable height may not be readily identifiable for a particular location unless some care is taken (see e.g., Namboothiri et al. 1993). However, it is possible that with care, the actual height can be determined, and there is also good evidence that winds above 100 km can be recovered at some times of the day and at some locations using MF/HF SA techniques (Namboothiri et al. 1994) and MF meteor methods (e.g., Tsutsumi and Aso 2005).

Given the issues around in the influence of the height of the total reflection, the selection of the operating frequency is very important. This is more so the case because of the proximity of the operating frequencies to those of the AM broadcast band, MF and HF amateur bands, radiolocation bands, and maritime communication and mobile communications bands. In most instances, the radar frequency is determined by the available spectrum

and licensing. The best operating frequency ( $f$ ) is a balance between the competing requirements of licensing, good backscattered power, which goes as  $1/f^2$ , and favors a lower frequency, and the reflection height, which goes as  $f$ , and favors a higher frequency. As a consequence of these limitations, current PR radars operate in the range from 1.94 to 3.18 MHz as shown in Table 2.

In addition to forming an upper limit to the upper measurement height of MF and lower HF radar techniques, strong E region returns may have another impact on winds above about 92 km during the middle of the day. Because of the long tail on the Gaussian transmitter pulses used, and the steep gradient in returned power in height approaching the E region, height gates well away from the height of the total reflection layer may be contaminated by returns from the E region, possibly making the derived winds unrepresentative, and potentially unusable. This was first suggested by Hocking (1997) in the context of finite receiver bandwidths and who suggested that this was most likely to be an issue around mid-day. He suggested that all data over a measured height of 92 km should be discarded and repeated this in a subsequent review (Hocking 2011). This conservative approach is appealing in its simplicity, and a safe approach, but may not be entirely necessary when with some effort, suspect data could be excluded from further consideration after initial processing.

As noted above, the influence of the E region represents an upper limit to the technique during daytime. The majority of investigators have taken the view that below about 100 km at mid-latitudes any group retardation effects are negligible, that the real and virtual heights are equivalent below 100 km, and E region contamination was minimal. As we have noted above, this is too lax. However, the quality control criteria applied within most analysis techniques mean that the quality of the data is high and that some results contaminated by total reflections are most likely omitted. This is one reason for the relatively high rejection rates above 90 km during the day (greater than 50 % in ordinary mode (O-mode) and greater than 75 % in E mode) as we shall see below. The current quality control parameters (or equivalently the rejection criteria) for the BPFM SA FCA are summarized in Table 6 by way of example.

However, there is no doubt that great care must be taken to avoid contamination from total reflection, and the addition of other quality control measures to address this is recommended. In addition, an active consideration of the likely total reflection height, the consequent restriction of data to unaffected height ranges, an active consideration of group retardation and a correction made for it, and the use of smaller range resolutions to increase the number of unaffected range gates at least above 90 km should be

implemented. At 2 MHz, a 2 km pulse oversampled to 1 km is suggested.

#### Character of the ground diffraction pattern

An example of a snapshot in time of a D region diffraction pattern from a weak partial reflection from a height of 80 km is shown in Fig. 6. This was obtained using the BPFM radar using a technique described by Felgate and Golley (1971), and further descriptions relevant to this are provided by Briggs and Holmes (1973), Holmes (1975), and Briggs (1993). It is the motion of this ground diffraction pattern that is used to infer the motion of the atmosphere at the partial reflection or backscatter height. In an attempt to do this by sampling the ground diffraction pattern at a limited number of locations, the various spaced antenna techniques that we discuss here were used. Generally, the number of locations sampled is limited by cost. If all of the pattern was available as it is in Additional file 2: Video 2, then in a modern radar system, image processing techniques could be applied to determine the motion of the pattern as is done for cloud images in both the lower and upper atmosphere (e.g., Rong et al. 2015). This does assume that all of the

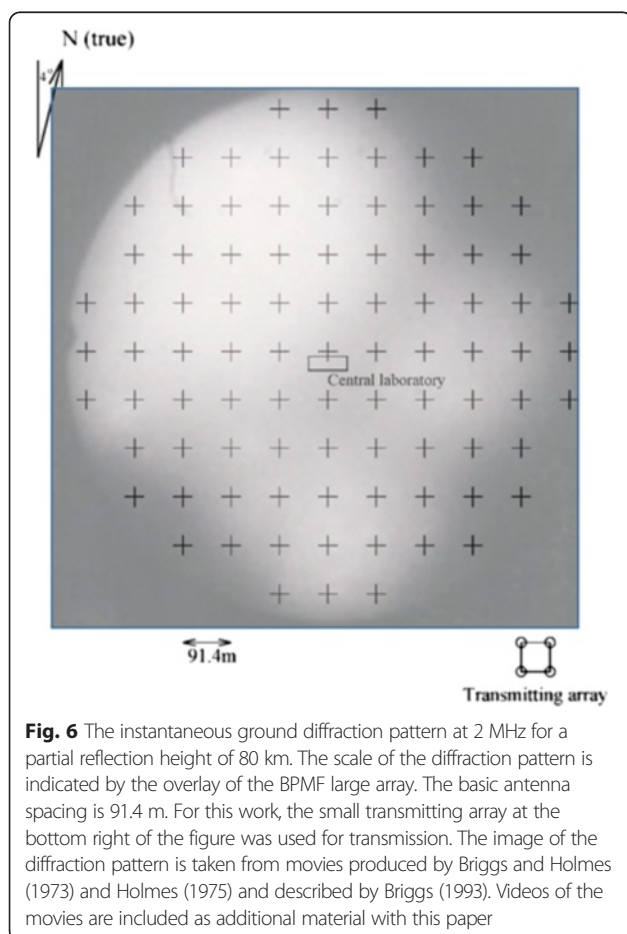
motion of the ground diffraction pattern is due to the horizontal motion of the atmospheric irregularities producing it, and this does not always hold true. For example, differential vertical motion in the radar pulse volume can induce an apparent horizontal motion of the pattern (e.g., Røyrvik 1983). We will return to this below. Additional file 2: Video 2 shows the sequence from which Fig. 6 was obtained. The fading shown in Additional file 1: Video 1 corresponds to the variation in the strength of the electric field at a particular position on the ground as the diffraction pattern moves over the receiving antennas.

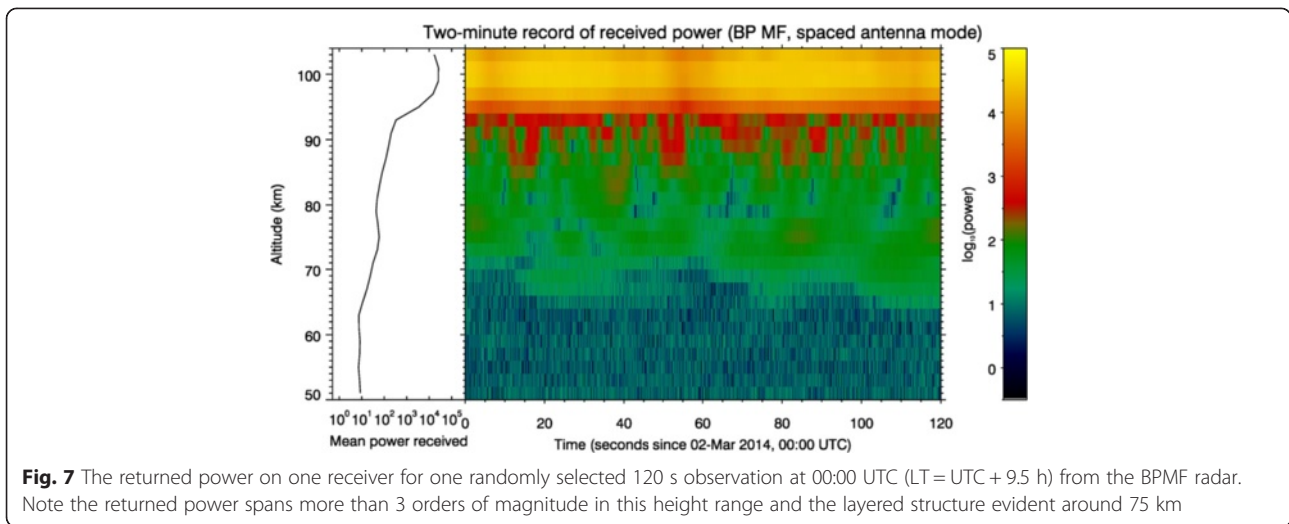
A more contemporary example of a SA data record is shown in Fig. 7. This shows the returned signal measured during a 120 s period every 0.4 s (after coherent integration) over a range of heights for a single receiver for the BPFM radar, along with the corresponding mean power profile. This figure shows the variation in power with height and the tendency to layering. The corresponding figure for this record showing the variation of the amplitude of the signal from each range gate (the fading) is shown in Fig. 8. In the simplest spaced antenna analysis, the signals detected at three spaced antennas corresponding to the fading shown in Fig. 7 are analyzed using a correlation analysis to determine the motion of the diffraction pattern of the partially reflected signal from the D region over the ground. The detection may utilize coherent receivers, but only the amplitude information is used in the analysis.

A schematic representation of the SA experiment is shown in Fig. 9 (MacKinnon et al. 2002). The ground diffraction pattern is sampled at three ground locations. In this case, which corresponds to the arrangement used at VHF for the boundary layer version of the SA experiment, groups of nine antennas are used for both reception and transmission. Groups of three or four antennas are similarly used at each received location with the BPFM radar with SA mode (see e.g., Holdsworth and Reid 2004a), and there is a consequent increase in gain and a high frequency filtering of the ground diffraction pattern in both cases.

Figure 10 shows a sequence of a few hours of the signal to noise ratio (SNR) for one receiver for the BPFM radar again showing the tendency for layering. In this example, sunrise occurred at 21:05 UT (6.35 am LT). The layer between 60 and 65 km that forms around sunrise is consistent with VLF observations of the C layer described by Bertoni et al. (2013) and mentioned above. The layer near 75 km is also commonly observed and, as discussed above, is often associated with a “preferred height”.

Figure 11 shows the height profile of the SNR for the Davis Station MF SA radar for one receiver for 1 year of observations for O mode (McIntosh et al. 2010). A distinction is often made between the nature of the scattering processes above and below about 80 km. In this context,





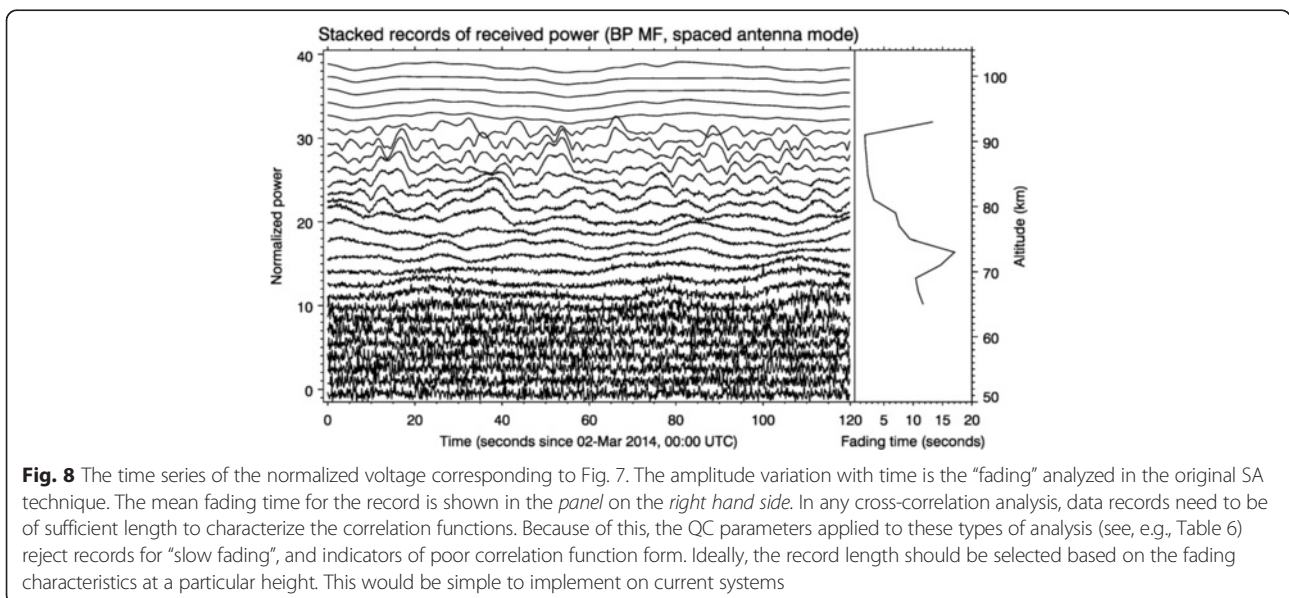
we note the rapid increase in SNR between 82 and 84 km, which corresponds to a gradient of about 8 dB/km. This rapid increase in returned power is the rationale for using two sampling regimes and two gain settings on some radars. Another example of a height profile of returned power for a brief period of observation is given in Fig. 4, in this case for the Saura HF radar in northern Norway. This example shows height profiles of both the O and X mode returned powers, which range over 65 dB.

Generally, slow fading times are associated with more aspect sensitive backscatter, and so with larger scales of the ground diffraction pattern. The aspect sensitivity is parameterized as the half width of the backscatter polar diagram and given by  $\theta_S$  (see e.g., Holdsworth and Reid 2004a). A review of the methods for investigating thin sheets of temperature gradients in the lower atmosphere

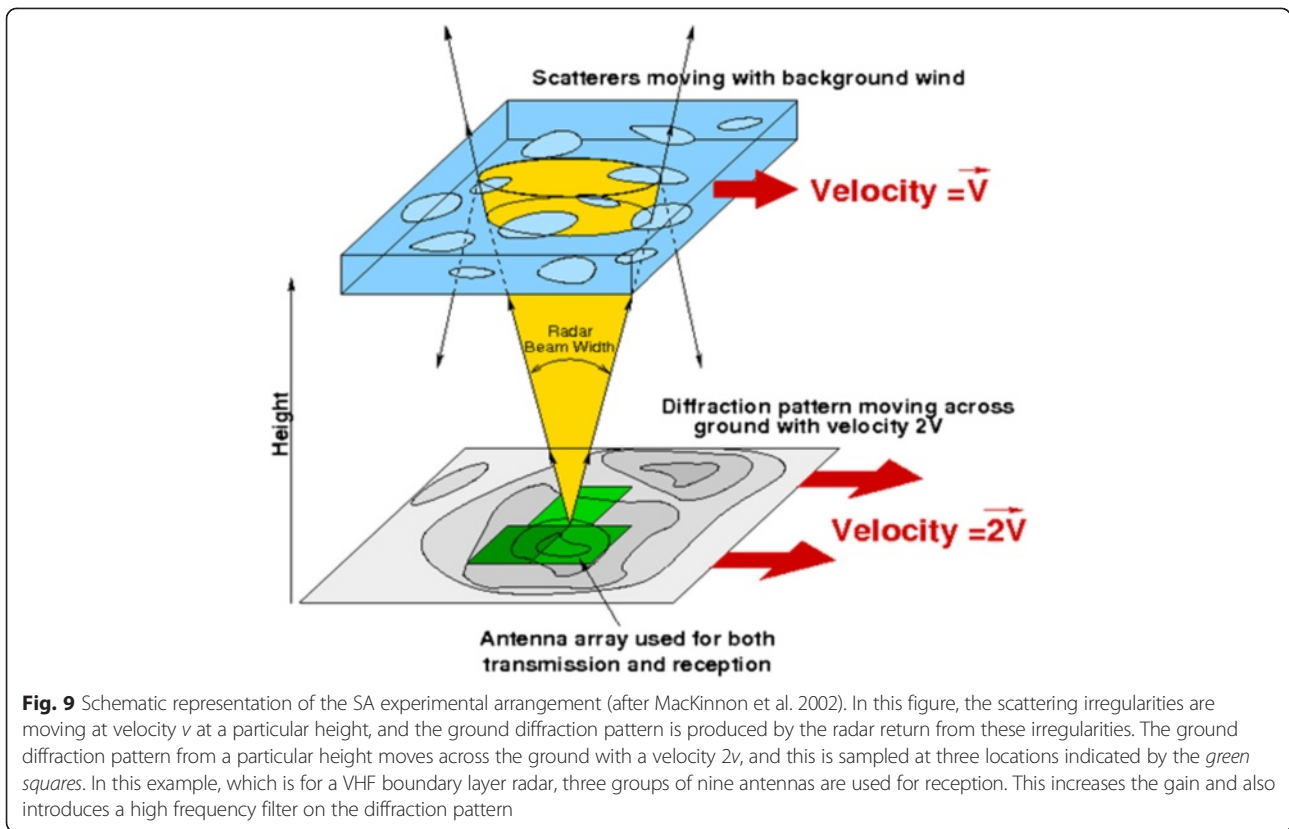
by Luce et al. (2001) provides a useful review of techniques for measuring aspect sensitivity and of the relationship between atmospheric structure and aspect sensitivity.

In addition to the rapid increase in power, there is a change in character of the backscatter at heights of around 80 km, from more to less aspect sensitive (Figs. 7 and 11). This suggests that one challenge of spaced antenna techniques is to adequately characterize the ground diffraction pattern through all sampling heights. This may not be possible when the same sampling scheme is used for all heights.

Hocking (1981) estimated that minimum data lengths of  $(80 - 100) \times T_{0.5}$ , where  $T_{0.5}$  is the fading time, are required to produce the true spectrum of velocities in the backscattering region. Inspection of Fig. 8, which is typical, suggests that data lengths of 160–500 s may be required





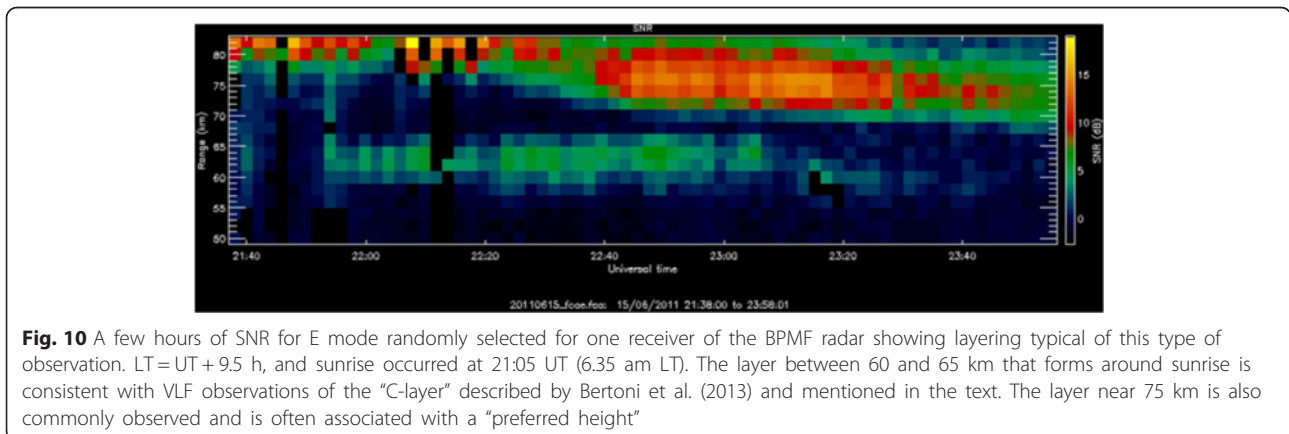


between 80 and 90 km and much longer lengths required above and below this height range. Typical data lengths used at Saskatoon were about 5 min (Meek and Manson 2001), but at Adelaide and many of the other radars in Tables 2 and 3, typical data lengths used for SA analyses were around 2 min, a length originally determined by computer limitations at the field site. Two minute record lengths are still typical, although now unnecessarily so, and the use of longer, fading time-dependent data record lengths is recommended. We note here that implicit in many of the SA analysis techniques, including the FCA, is the assumption of volume scatter. If discrete scattering

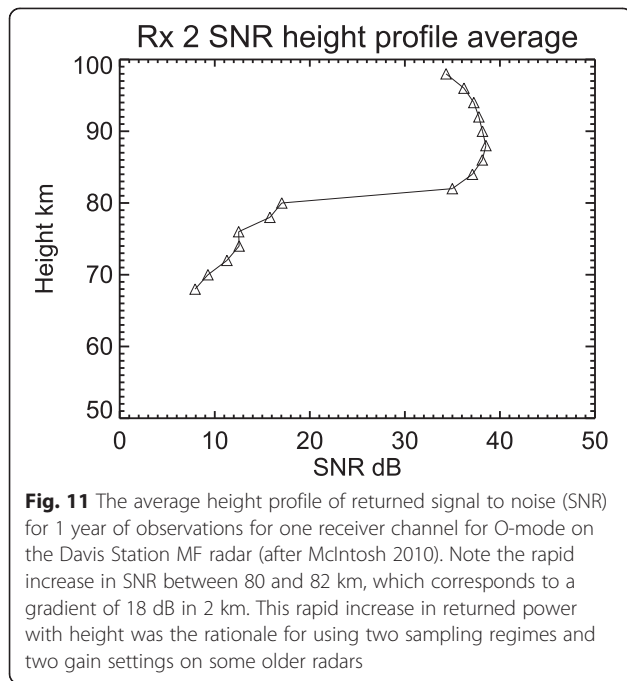
targets exist, then interferometric techniques could measure radial velocities in shorter time intervals than indicated by Hocking’s analysis. We will return to this point below and discuss the formation of the ground diffraction pattern when we discuss DBS techniques.

*Spaced antenna analysis techniques*

**Similar fades** The oldest and simplest analysis technique for spaced antenna data is the “method of similar fades” (see e.g., Mitra 1949; Krautkrämer 1950; Sprenger and Schminder 1969). This approach involves measuring







and recording the fading of a radio signal returned from the ionosphere at three points on the ground at the corners of a triangle. The receiving locations are separated by distances of the order of one wavelength or less. Originally, the triangle was right-angled, but this was later shown to introduce a bias into the derived velocity, and subsequently, equilateral triangles were generally used (Stubbs 1973). The velocity of the ground diffraction pattern is then determined from the time displacements of the fading measured at each receiving location. A simple correction is made for the point source effect (the derived velocity is divided by two; see Felgate 1970; Briggs 1980). A series of experiments in the late 1960s and early 1970s determined that the motion of the ground diffraction pattern could be well characterized using only three non-collinear receiving locations (Briggs 1980; 1994). Varieties of this spaced antenna analysis all attempt to determine the motion of the atmosphere from the same basic information provided by the ground diffraction pattern. We will return to this below.

It was realized very soon after the introduction of the simple “similar fades” analysis that a complete evaluation of such measurements needed to take into account the effects of any random changes and any anisotropy of the ground diffraction pattern as it moves across the receiving antennas. An analysis to do this was developed by Briggs et al. (1950), Phillips and Spencer (1955), Ratcliffe (1956), and others and called the FCA method. A more contemporary description is given by Briggs (1984) and Holdsworth and Reid (1995a). However, as explained by Sprenger and Schminder 1969, at that time the FCA was

relatively laborious and expensive, and so the simple similar-fade method was often preferred. They also describe another approach used with similar fades. This was to average the “drift” vectors measured between the spaced receiving locations to determine the velocity of the ground diffraction pattern.

When a simple correlation analysis (effectively a similar fades analysis) is used to determine the movement of the ground diffraction pattern across three non-collinear antennas, the resulting velocity does not take into account random changes in the pattern as it moves, or any anisotropy in the pattern. This results in a velocity that overestimates the magnitude of the true velocity. For this reason, this velocity is called the “apparent” velocity in the FCA. This is illustrated in Fig. 12 which is taken from Briggs (1993). Part (a) of this figure illustrates a changing pattern  $E(x, t)$  moving past two antennas separated by distance  $\xi_0$  with velocity  $V$  to produce records  $E_1(t)$  and  $E_2(t)$ . Part (b) shows the cross-correlation function  $\rho_{12}$  that takes a maximum value a lag  $\tau_m$ , smaller than the “correct” value  $\frac{\xi_0}{V}$  because of these

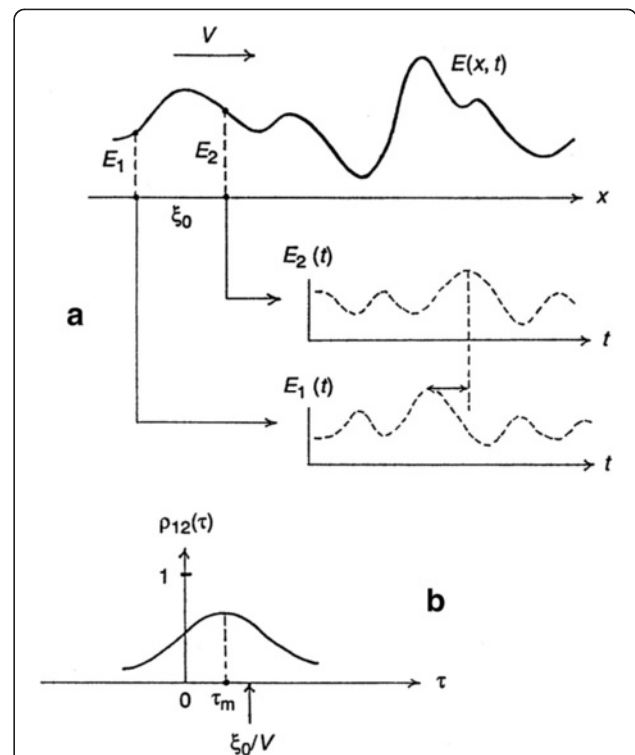


**Fig. 12** (After Briggs 1993) Part a of this figure illustrates a changing pattern  $E(x, t)$  moving past two antennas separated by distance  $\xi_0$  with velocity  $V$  to produce records  $E_1(t)$  and  $E_2(t)$ . Part b shows the cross-correlation function  $\rho_{12}$  calculated from  $E_1(t)$  and  $E_2(t)$  that takes a maximum value a lag  $\tau_m$ , smaller than the “correct” value  $\frac{\xi_0}{V}$  because of these changes, and consequently, an overestimation of the correct velocity  $V$ , the “apparent” velocity  $V_a$  is produced

changes, and consequently an overestimation of  $V$ , the apparent velocity. It is easy to understand how this comes about if we consider the limiting case of  $V=0$  and only random motions. In this case, the maximum cross correlation will be at  $\tau_m = 0$ .

Sprenger and Schminder (1969) argued that the simple similar fades approach produces a result very similar to the “apparent velocity” derived in the FCA method, whereas the velocity obtained from averaging the drift vectors produces a result in a term more similar to the “true velocity” in the FCA method. In this, the technique is similar to the simplest imaging Doppler interferometer (IDI) techniques, which we discuss below, and which produce a term similar to the apparent velocity.

The similar fades spaced antenna analysis using the drift vector approach was applied at LF and oblique incidence using commercial radio transmitters about 165 km distant from the receiving site in Germany from 1959 until 2007, with height information being available from 1982 onwards. This approach is effectively a single height measurement, with the mean reflection height being typically 90 to 95 km, and the measurements were restricted to nighttime because of strong daytime absorption. A description of the experiment, the analysis and results is given by Schminder and Kürschner (1994).

#### Full correlation analysis

Like the method of similar fades, the FCA utilizes a minimum of three spaced antennas to sample the ground diffraction pattern produced by the backscattering irregularities. Table 4 shows the typical operating parameters for the BPFM radar operating in SA mode. Cross correlation techniques are used to determine its

**Table 4** Experimental parameters used for routine Spaced Antenna FCA for the Buckland Park MF radar

Parameter	Day value	Night value
Start range, km	50	70
Range resolution	26.6 $\mu$ s (4 km)	26.6 $\mu$ s (4 km)
Sampling range resolution, km	2	2
Number of ranges	25	15
Polarization	Linear	Linear
PRF, Hz	100	40
Coherent integrations	40	16
Effective sampling time, s	0.4	0.4
Number of complex samples	280	280
Record length, s	112	112

A typical 112 s data record is shown in Fig. 7. In common with most modern radar techniques, it is suggested that coherent integration should be avoided. Also, as discussed in the text, it is suggested that the sampling times and record lengths be better matched to the characteristics of the fading at each sampling height

velocity of motion, and the analysis takes account of random changes in the pattern, and also any anisotropy of the pattern, so that both horizontal components of the wind field are measured at a particular height in a single region directly above the radar. This analysis yields the horizontal wind velocity, as well as a number of parameters related to the ground diffraction pattern itself. These are summarized in Table 5. The analysis was originally applied to amplitude only time series data, but current systems all use coherent data acquisition systems. However, the FCA itself does not make full use of the phase information available. The apparent vertical velocity, angle of arrival (AOA), and corrected vertical velocity in this table are calculated outside of the FCA.

The FCA is the most common analysis routinely applied to spaced antenna radars. It has been routinely applied at MF to investigate the atmosphere in the 60–100 km height region since the early 1970s on a campaign basis (e.g., Stubbs 1973), then as a continuous and routine real-time measurement of the MLT region (Gregory et al. 1979; Meek 1980). This development continued and in the early 1990s, commercial three or four receiving antenna MF/HF SA radar systems became available for the first time, and a de facto antenna arrangement standard as shown in Fig. 2 for small partial reflection MF/HF radars using the FCA was established.

However, a variety of transmitting and receiving antenna arrangements were and are still common, particularly with older larger systems established for the DAE or as large general purpose antenna arrays. For example, at Saskatoon, a vertically pointing  $4 \times 4$  array of folded half-wave dipoles with a half-power beam width of about  $15^\circ$  operating at 2.219 MHz was used for transmission. Either four half-wave receiving antennas spaced at  $1.16\lambda$  and arranged in a “Y” arrangement or three half-wave dipoles arranged in a triangle with a spacing of  $1.35\lambda$  were available for reception for routine observations (see e.g., Meek and Manson 1987). At Adelaide, a square array of four half-wave dipoles was used until the early 1990s for transmission, and three groups of four half-wave dipoles were used for reception for routine observations (see e.g., Stubbs 1973).

Such arrangements affect the sampling of the ground diffraction pattern by performing a spatial average on it by removing finer scale structure. This is equivalent to restricting the angles of arrival of the backscatter detected by using narrower polar diagrams on reception. This means that the filtering of the ground diffraction pattern is different on different antenna systems, and this may potentially influence the results of the analysis.

The height coverage of MF/HF PR radars is amongst the best available from typical upper atmospheric radar systems. By way of example, typical acceptance results for 2 min records for both O and E modes, and for day

**Table 5** Parameters derived from the SA FCA

Symbol	Parameter	Description
$V_a$	Apparent velocity	The velocity of the ground diffraction pattern over the spaced antennas calculated from the time delays of the cross-correlation function determined between pairs of antennas.
$V_t$	True velocity	The velocity of the ground diffraction pattern over the spaced antennas calculated from the time delays of the cross-correlation function determined from pairs of antennas corrected for random changes in the pattern in time and for any pattern anisotropy. Additional quality control parameters are also applied to obtain this parameter (see Table 6).
$w_a$	Apparent vertical velocity	Vertical velocity measured from the phase of the complex autocorrelation function measured on each antenna uncorrected for angle of arrival
$w_{cor}$	Corrected vertical velocity	Vertical velocity corrected for effects of off-zenith mean angle of arrival
AOA	Mean angle of arrival	Mean angle of arrival
$\tau_{0.5}$	Fading time	Mean auto-correlation function half-width
$T_{0.5}$	Pattern lifetime	Fading time in the frame of the ground diffraction pattern
$S_{0.5}$	Pattern scale	Major axis of the characteristic ellipse
$R_{ax}$	Axial ratio	Ratio of the major to minor axes of the characteristic ellipse
$\theta_{ax}$	Axial rotation	Direction of major axis of characteristic ellipse
PTD	Percentage time discrepancy	Ratio of sum of cross-correlation function maximum delay times to sum of absolute cross-correlation function delay times
SNR	Signal to noise ratio	The signal to noise ratios for each receiver channel
$P$	Received power	The received power for each receiver channel

and night, are shown in Figs. 13 and 14 for routine FCA operation of the BPFM radar. These results correspond to a 3 year period of observation, and the acceptance criteria applied are those shown in Table 6. Daytime O mode acceptance rates peak at around 70 % near 82 km and acceptance rates for X mode peak at about 40 % near 71 km. During nighttime, O mode rates peak at around 40 % near 88 km, and X mode around 50 % near 84 km.

The FCA has also been applied at other frequencies. It was first applied at VHF to measure wind velocities in the 2–20 km height region in the mid-1970s (Vincent and Röttger 1980). Since the mid-1990s, it has been applied at VHF to mesospheric data using MST radars (e.g., Morris et al. 2006) and to boundary layer data using 55 MHz radars (0.3 to 8 km) (e.g., Dolman and Reid 2014), and at ultrahigh frequency (UHF) (Dolman and Reid, private communication, 2015).

It has proven to be a reliable and robust analysis but does underestimate the magnitude of the wind velocity. In general, any noise in the FCA analysis will lead to an underestimate of the derived wind velocity. This has been investigated extensively using a numerical model by Holdsworth and Reid (1995a, 1997). In addition, there is a tendency for the derived velocity to be too small if antennas are too closely spaced, the so-called triangle size effect (TSE), if the sampling rate is too low, if there is receiver saturation, if there are digitizer quantization errors, or if there are channel differences associated with antenna matching or receiver phase characteristics (see e.g., Holdsworth 1999).

When all of these effects are taken into account, there is still an underestimation of the wind magnitude. Holdsworth and Reid's modeling and their work using the BPFM radar suggested a 10 % magnitude underestimation at MF/HF. For some small MF/HF systems, the underestimation is found to be up to 15 to 40 % and strongly height dependent. For comparison, it is typically up to 5 to 10 % at VHF and only weakly height dependent, if at all (e.g., Reid et al. 2005; Dolman and Reid 2014). It is likely that antenna system mismatches play some role in the larger underestimation at MF/HF for modern systems, and this is an important aspect of maintenance for such systems, particularly after some years of operation. However, antenna mismatches cannot explain the height dependence of the bias. We return to this below.

An example of a wind intercomparison between a small MF/HF SA FCA radar and a meteor radar is shown in Fig. 15. These data represent 1 year of observations from a 2 MHz MF PR SA radar which has an arrangement similar to that shown in Fig. 2 and the 33 MHz "all-sky" meteor radar at Davis Station in Antarctica (McIntosh et al. 2010). This is for a height of 88 km, which is near the peak meteor count rate, and also generally corresponds to the highest acceptance rates for the MF winds at this location. The red and blue lines indicate least-squares fits of MF on meteor, and meteor on MF winds respectively, and so are the bounds of the fits assuming errors in only one technique. The dashed line indicates  $y = x$ , and the green line indicates

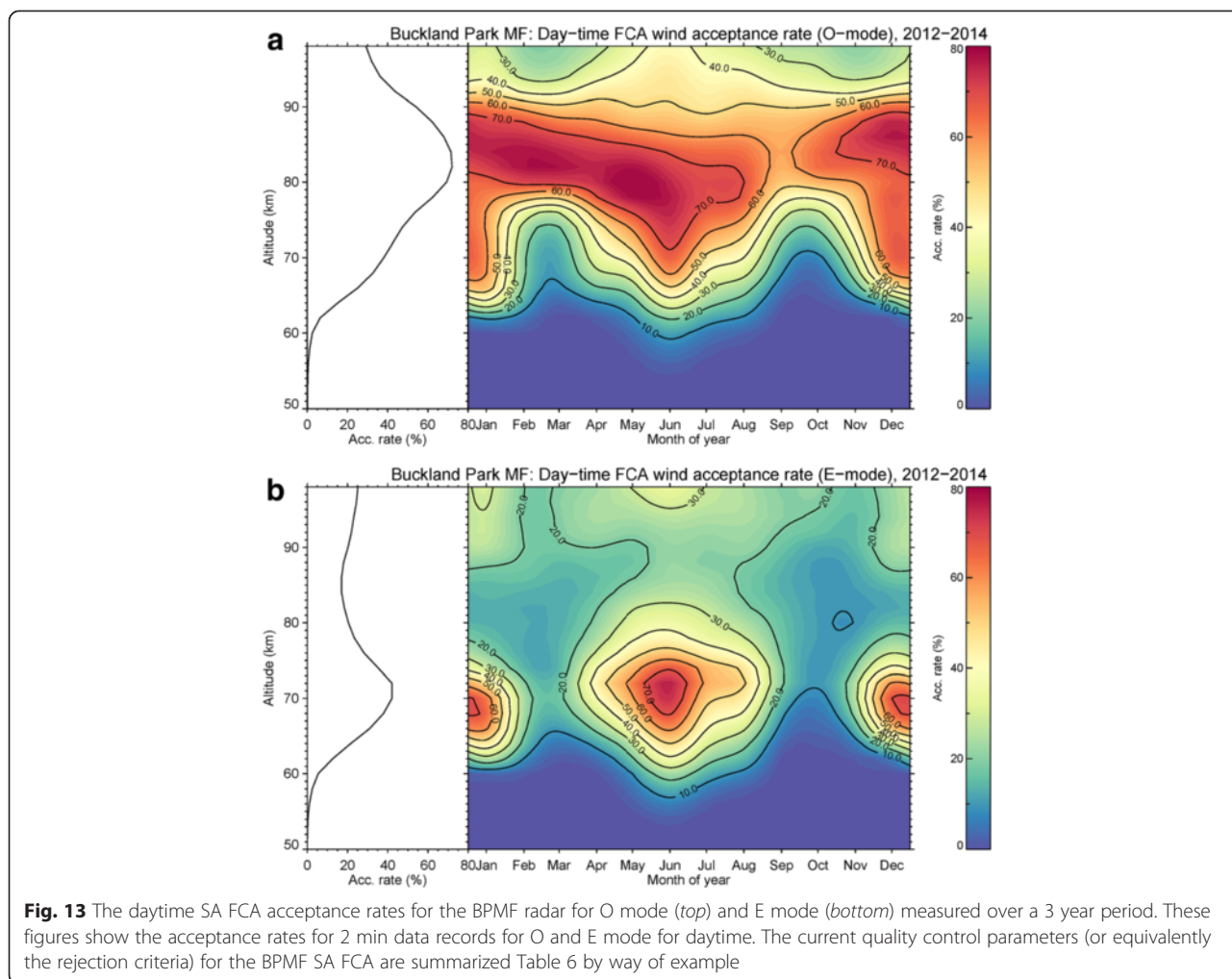


**Fig. 13** The daytime SA FCA acceptance rates for the BPMF radar for O mode (top) and E mode (bottom) measured over a 3 year period. These figures show the acceptance rates for 2 min data records for O and E mode for daytime. The current quality control parameters (or equivalently the rejection criteria) for the BPMF SA FCA are summarized Table 6 by way of example

the slope of fit after estimating the actual errors in each technique. The purple line represents the slope derived using error values obtained for the meteor radar from a similar comparison of the 55 and 33 MHz meteor radars at the same site. This analysis indicates the MF winds underestimate of the meteor winds in the zonal component, with a value of 0.82, with the corresponding meridional value being 0.77.

In this context, it is interesting to note that Dolman and Reid (2014) have described an empirical correction for the bias on operational boundary layer tropospheric (BLT) VHF SA FCA wind profilers. The form of their correction was determined by extensive intercomparison with radiosonde winds and appears to be very robust. With a suitable technique on which to base an intercomparison, it should be possible to also correct for the magnitude bias evident in the MF/HF SA FCA winds. However, it should be noted that unlike the FCA correction for VHF SA radars, experience shows that the MF/HF FCA correction is likely to be strongly height dependent and that there are few options for intercomparison techniques below about

80 km. Needless to say, bias correction will not remove the effects of E region contamination.

Just why the underestimation is height dependent is a question that still needs to be addressed. There are a number of possibilities, including inadequate sampling of the ground diffraction pattern. The ideal antenna spacing for the FCA is that for which the cross-correlation values are typically one half. We have seen how slower fading is associated with smaller values of the aspect sensitivity parameter ( $\theta_S$ ) and with a larger pattern scale. We have also seen how the fading times change with height and the sharp demarcation between the character of the fading and signal powers at heights near 80 km during the day. This means that the antenna spacing cannot be matched to the diffraction pattern scale for every height. The use of the arrangement shown in Fig. 2 does help because there is more than one basic spacing, but this does seem to be a fundamental issue when using the FCA. Furthermore, when a fixed sampling rate and record length are used for all heights, it is probable that this is better suited to some heights than



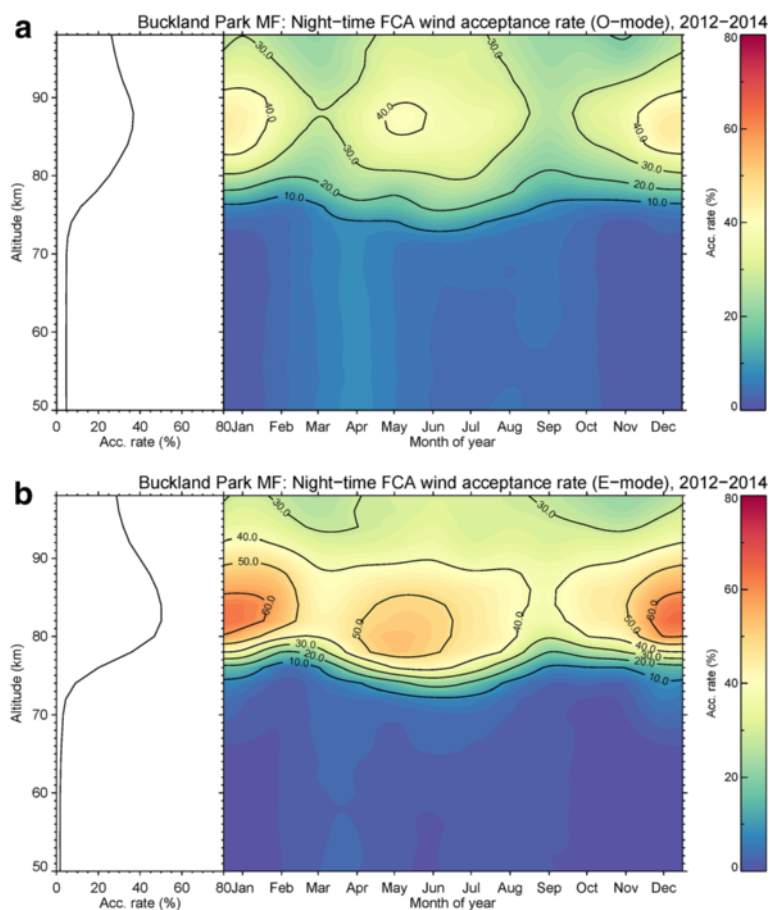


**Fig. 14** The nighttime SA FCA acceptance rates for the BPMF radar for O mode (top) and E mode (top) measured over a 3 year period. These figures show the acceptance rates for 2 min data records for O and E modes for nighttime

others. Dolman and Reid (2014) did note a weak dependence on wind speed, again suggesting a sampling issue. In the MLT region, large vertical shears in magnitude are common, and so, the quality of the characterization of the ground diffraction pattern may also be height dependent. Modern systems have the ability to vary their sampling schemes with sampling height, and this should be investigated.

Dolman and Reid (2014) also describe a quality control (QC) approach for the winds derived from the FCA analysis. QC at the spectral level is not an option for SA radars running the FCA technique as it is for DBS radars, and outliers must be identified in the wind profiles themselves. Dolman and Reid (2014) follow Weber and Wuertz (1991) in developing a successful QC technique for SA FCA-derived winds. This raises the question of whether MF/HF SA FCA winds should be quality controlled. Of course, this is the norm for most observing systems (e.g., satellite-based instruments), and since most radars are now operated more as turnkey wind

measuring systems, rather than as pure research radars, this seems appropriate.

Additional information that can be recovered from the FCA analysis relates to the turbulent velocity and the aspect sensitivity and general form of the scattering irregularities.

**Turbulent velocity**

The basic theory of turbulence velocity estimation using the FCA is described by Briggs (1980), and examples of its application are provided by Holdsworth et al. (2001) and Holdsworth and Reid (2004a). Holdsworth et al. (2001) demonstrated that wider transmit beam widths lead to an overestimation of the turbulent velocity. This confirmed the suggestions made by previous authors (e.g., Briggs 1980; Vandepier and Hocking 1993; Hall et al. 1998). They concluded that using relatively narrow transmitter beams (in their case, the BPMF radar operated with transmit beam half-power widths of 9°) reduced the effects producing



**Table 6** Quality control criteria for the FCA of the SA experiment

Code	Meaning
0	No error—analysis result ok.
1	Time series unsuitable for analysis (signal amplitude too low or interference present)
2	Signal to noise ratio < -3 dB
3	Fading time >6 <sub>s</sub>
4	At least one cross-correlation function maxima lies outside end points
5	Percentage time discrepancy >35 %
6	$V_c^2 < 0$
7	Ground diffraction pattern analysis breaks down
8	Apparent velocity magnitude $V_a > 400 \text{ ms}^{-1}$ True velocity magnitude $V_t > 200 \text{ ms}^{-1}$
9	Difference between apparent $V_a$ and true $V_t$ direction exceeds 40°.
10	$V_a > 10V_t$
11	$V_t > 1.5V_a$
12	Poor fit to cross-correlation function (CCF) maximum
13	At least one CCF maximum <0.2
14	Poor zero-lag auto-correlation function (ACF) interpolation
15	Insufficient number of lags on main peak of mean auto-correlation function (MACF) to estimate fading time
16	Poor fit to MACF
17	Secondary maxima in MACF >0.5 (oscillatory)
18	Mean ACF >0.5 at end lags
19	One or more CCF maxima exceeds 1.0

overestimation of turbulent velocities and resulted in a usable result. Holdsworth and Reid (2004a) later showed that turbulent velocities derived using the IDI technique were equivalent to those from the FCA.

The FCA estimate of the turbulent velocity is given by

$$v_{FCA} = \frac{\lambda \sqrt{2 \ln 2}}{4\pi T_{0.5}},$$

where  $\lambda$  is the wavelength and  $T_{0.5}$  is the ground diffraction pattern lifetime in the reference frame of the pattern (e.g., Holdsworth et al. 2001). Figure 16 shows the turbulent root mean square velocities obtained by Holdsworth and Reid (2004a) for a period of 7 years using the BPMF radar. Turbulent velocities are observed to increase with height and solstitial maxima and equinoctial minima are observed below 80 km. Inspection of this figure indicates that there is a maximum extending from 93 km in summer to above 98 km in winter. Holdsworth and Reid (2004a) attribute this to contamination from the E region total reflection because routine harmonic analysis of the turbulent velocities at these heights and times yields values which peak at mid-day when the E region contamination is expected to be most likely (e.g., Holdsworth et al. 2001)

**Aspect sensitivity**

The FCA also allows an estimate of the aspect sensitivity  $\theta_S$  of the backscattering irregularities to be estimated as (Lesicar et al. 1994; Holdsworth and Reid 1995a)

$$\begin{aligned} \sin^{-2} \theta_S &= \sin^{-2} \theta_{S0} - \sin^{-2} \theta_0, \text{ with } \theta_{S0} \\ &= \frac{15.2 \lambda \sqrt{R_{ax}}}{S_{0.5}} \end{aligned}$$

and where  $S_{0.5}$  is the pattern scale,  $R_{ax}$  is the axial ratio,  $\theta_{S0}$  is the  $1/e$  half width of the effective polar diagram of the backscatter including the antenna polar diagram. Figure 17 is from Holdsworth and Reid (2004a) and shows the mean aspect sensitivity calculated for a 7 year

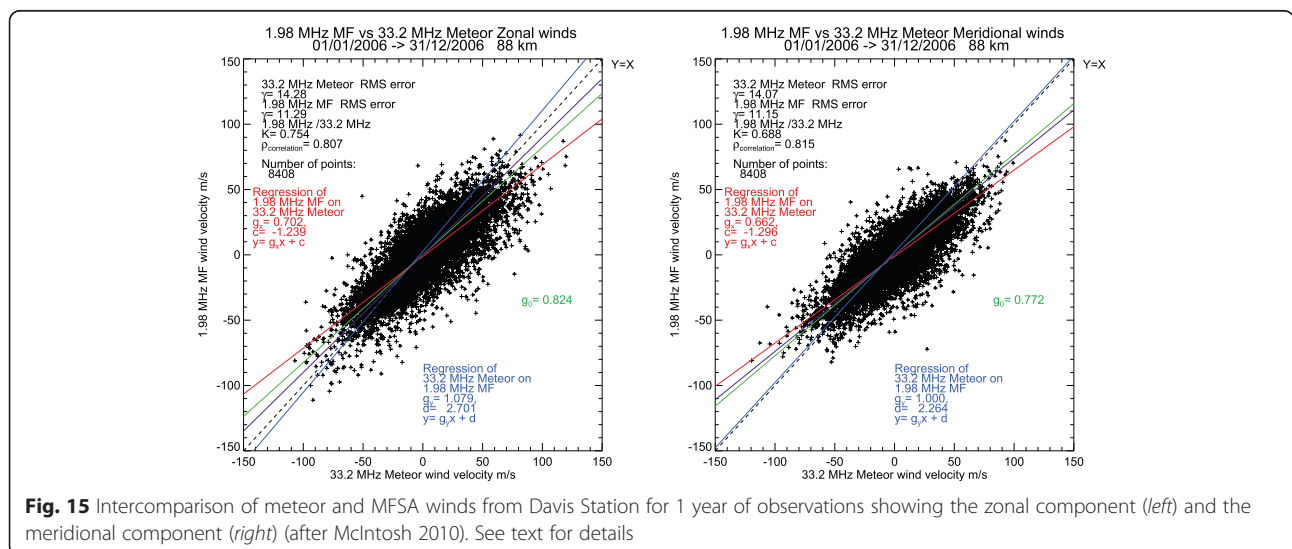


**Fig. 15** Intercomparison of meteor and MFSA winds from Davis Station for 1 year of observations showing the zonal component (left) and the meridional component (right) (after McIntosh 2010). See text for details

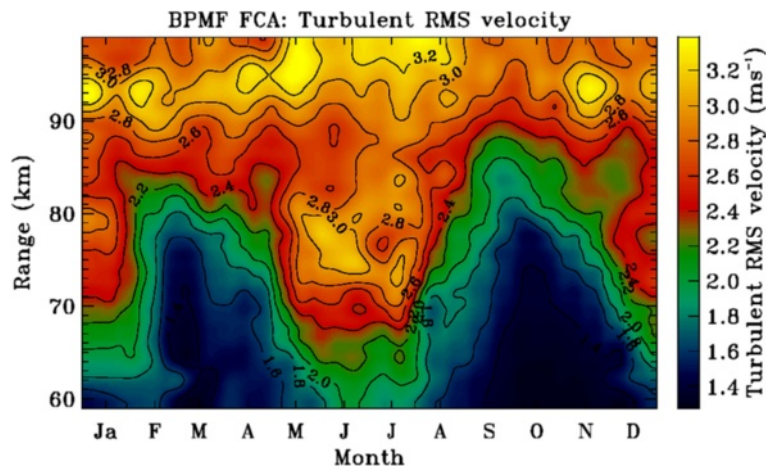


**Fig. 16** The turbulent root mean square velocity measured at Buckland Park for a period of 7 years using the spaced antenna technique and the full correlation analysis (after Holdsworth and Reid 2004a)

period at 2 MHz for the BPMF radar derived using this technique. Inspection of this figure illustrates a general increase in the aspect sensitivity with decreasing height, and a seasonal variation, with the least anisotropic scatter occurring above 80 km in winter. The backscatter is different in character above and below about 80 km, with scatter from a range of angles up to about 10° to 15° centered on the zenith above 80 km, indicating a mixture of quasi-isotropic and specular scatter, while below, scatter is from a more restricted range of angles, typically less than 5°, indicating a scattering process rather more specular in character.

**Imaging Doppler interferometry**

There are a number of interferometric analyses available for use with spaced antenna systems, and Chau (2000)

provides a good review. The most commonly applied at MF/HF is IDI. The raw data acquired by the IDI and other SA techniques are essentially identical. However, as in all interferometry, multiple antenna spacings are desirable in order to reduce the possibility of ambiguity in the phase corresponding to the angle of arrival of the returned signal, when the spacing is larger than a wavelength (by also using a spacing less than a wavelength), while reducing the uncertainty in the phase (by using a larger spacing). This requirement perhaps gives some insight into the limitations imposed on the sampling of the ground diffraction pattern by the fixed antenna spacing used by current small MF/HF FCA systems. The IDI and non-interferometric SA techniques also differ in the assumptions they make about the backscattering medium, and consequently, in the subsequent analysis, and in that,

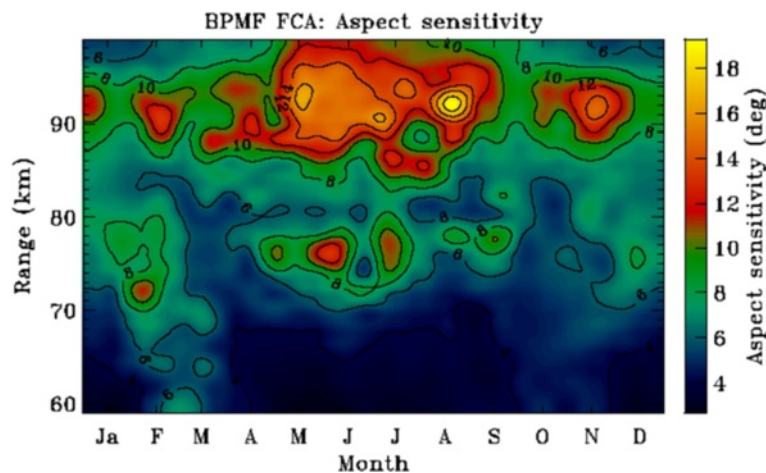


**Fig. 17** The aspect sensitivity  $\theta_5$  for 2 MHz for Buckland Park for a period of 7 years measured using the spaced antenna technique and the full correlation analysis (after Holdsworth and Reid 2004a)

IDI makes use of the available phase information. IDI-like techniques assume that discrete scattering regions exist in the atmosphere. The other non-interferometric SA techniques assume volume scatter.

The aim of IDI technique is to track individual radio wave scatterers in the neutral atmosphere, and it was first applied at MF (Adams et al. 1986). The experimental setup utilizes spaced antennas to sample the radio waves partially reflected or backscattered from the atmosphere. The analysis then looks for evidence of down-coming plane wave radiation and uses spectral techniques to locate a scattering position for each frequency bin. A radial velocity is associated with each scattering position, and the entire wind field can then be reconstructed. This approach has some similarity to the analysis of all sky meteor radar data but tends to require more scattering centers to derive a stable result in practice.

The fundamental assumption of IDI is that the phase information at each Doppler frequency results from a single discrete scattering location, but this original underlying theory of its operation is suspect (see Briggs 1995; Holdsworth and Reid 2004b).

The simple IDI analysis was extended by Franke et al. (1990) to remove the “single scatterer” criterion and the associated limitations regarding antenna configuration. They also introduced rejection criteria to quality control the data. These included limiting the acceptable range of zenith angles for angle of arrival data and setting limits on acceptable radial velocities. Without these, the IDI-derived velocities appeared to be the FCA apparent velocities (or equivalently, the similar fades velocities), a result predicted by Vandeppeer and Reid (1995a).

In this context, it is noteworthy that Pfister (1971) anticipated this result. He applied the SA experiment arrangement to E region radar returns in what seems to be the first attempt to make use of the phase information in the returned signals using this technique. He found that the phase of the cross-spectral functions measured between the spaced receivers was a linear function of the associated Doppler velocities of the reflecting surface, and he used the slopes of these phases to estimate the horizontal velocity of the surface. In doing so, he found that the interferometric wind velocities were in good agreement with the velocities obtained with the method of similar fades. While the Pfister (1971) results are for total ionospheric reflections, Bennett and Dyson (1993) later showed that this result generally applied when fixed ground sites were used to observe an ionosphere that moved without change of shape. This means that the same conclusions that apply to simple IDI in the MLT, namely that similar-fade apparent velocities correspond to the case for which changes in the backscatter, or equivalently, in the ground diffraction pattern over time, are not adequately accounted for, apply to the case of total reflections from the ionosphere.

Holdsworth and Reid (2004a) further investigated the IDI technique using a 3 year data set. They applied essentially the same analysis as that of Frank et al. (1990), but used the BP MF radar, which has a much narrower beam than the standard SA arrangement. In this special case, they found that IDI and FCA winds are comparable and concluded that IDI is a useful technique with three distinct and significant advantages over the FCA. The first is that it is significantly simpler to apply than FCA, requiring fewer criteria to reject bad data. The second is that it yields considerably higher 2 min acceptance rate percentages. The third and most important is that they found that the IDI velocities were around 10 % larger than FCA true velocities and in good agreement with spatial correlation function (SCA; see below) and hybrid Doppler interferometer (HDI; see below) velocities, which are better agreement with the actual wind velocity. That is, the magnitude bias evident in the FCA was not evident in the IDI technique in this special case.

One apparent disadvantage to IDI when compared to other non-interferometric SA techniques is that accurate phase calibration is required. However, it should be noted that the phase calibration of SA radars running the FCA analysis is also essential as discussed by Holdsworth and Reid (1997). They found in simulations using the Holdsworth and Reid (1995b) model that even small phase differences between the receiver channels resulted in an underestimation of the actual wind magnitude. The conclusion here then is that phase calibration is as important for SA radars running the FCA analysis as it is for those running the IDI analysis, and Holdsworth and Reid (2004a) describe how phase calibration is conducted periodically for the BPMF radar.

Briefly, Holdsworth and Reid (2004a) followed the approach of Golley and Rossiter (1970) and used a commercially available eight-way splitter to equally divide the signal received by a single antenna into multiple receivers. They did this manually at regular intervals as part of routine maintenance of their radar. They then calculated the cross-correlation functions (CCFs) of the resulting signals, and after interpolating across zero-lag to remove the effects of noise correlated between receiver channels (e.g., Briggs 1984), the zero-lag CCF magnitudes were estimated to measure the statistical similarity of the receiving channels. The zero-lag CCF phases were estimated to measure the phase difference between channels.

Holdsworth and Reid (2004a) do note that the technique they describe does not account for complex receiver gain variations that may occur over smaller time scales (e.g., diurnal variations as found by Vandeppeer and Reid 1995b in older radar equipment). It also does not account for antenna differences. It would be possible to supplement the Holdsworth and Reid (2004a) approach to apply an active automated self-calibration technique for the

entire receiver chain from antenna to digitizers as is done for meteor radar interferometers (e.g., Holdsworth et al. 2004b; Younger et al. 2013), and this approach is recommended using either meteor echoes or attenuated returns from the E region.

In summary, in spite of the issues around the actual form of the backscatter from the MLT region, IDI has been successfully applied by Franke et al. (1990) and Holdsworth and Reid (2004b) on SA MF/HF radars and also on MF/HF dynasonde radars to produce usable wind velocities (Jones et al. 1997; Jones et al. 2003). It makes better use of the phase information available than the FCA and is not susceptible to the underestimation bias of the FCA. With a radar with a suitably narrow transmit beam ( $\sim 9^\circ$  half-power full-width) and good phase calibration, it would be preferable to the standard FCA analysis.

#### **Other SA analysis techniques**

There are a number of other analysis approaches which are not routinely applied at MF and lower HF, but which are worth noting.

#### **Full spectral analysis (FSA)**

The full spectral analysis (FSA) is a variation of the FCA that differs from it in that the analysis takes place in the frequency, rather than time domain (e.g., Briggs and Vincent 1992; Holdsworth and Reid 1995b). This has some advantages, but the simple implementation of the technique at MF does not appear to be as robust as the FCA (Holdsworth and Reid 1997). Further development of the technique is described by Holloway et al. (1997) and by Venkatesh and Frasier (2013).

#### **Spatial correlation analysis (SCA)**

The SCA originated with Briggs et al. (1969). It determines the displacement of the ground diffraction pattern using the spatio-temporal autocorrelation function. When more than three receiving sites are used, it has some advantages over the FCA technique (Holdsworth and Reid 1995b, 1997). In particular, it is less susceptible to the triangle size effect and does not suffer from the magnitude bias evident in the FCA winds. It is noteworthy that the antenna arrangement shown in Fig. 2 does support analysis using the FCA, FSA, IDI, SCA, time domain interferometry (TDI), and meteor techniques, as well as the DAE and DPE experiments.

#### **Time domain interferometry (TDI) and hybrid Doppler interferometry (HDI)**

A problem when using the broad beams associated with the SA technique is that measurements of the vertical velocities are compromised because the mean angle of arrival of the backscatter is not typically from the vertical and so

has large uncertainties. In TDI (Vandepier and Reid 1995b), complex time series from spaced receivers are analyzed using the zero lag cross-correlation phase measured between multiple antenna pairs to determine a single angle of arrival of the backscatter from each data record. The average radial velocity measured from the autocorrelation functions of the time series sampled from each of the antennas can be associated with the mean angle of arrival to yield the average motion along the line of sight.

In the case of vertically directed beams, this can be used to calculate the vertical velocity and in the case of off-vertical beams, to determine the effective beam direction corresponding to the measured radial velocity. Because of their small relative magnitudes, vertical velocity measurements are always challenging. Furthermore, the apparent bias towards downwards vertical velocities observed in atmospheric radars with vertically directed Doppler beams has led to the results being treated with some suspicion.

Consequently, even when TDI is applied, vertical velocities obtained with MF/HF SA radars have been little used. Insight into the vertical bias, at least in the convective boundary layer, has been provided by Muschinski and Sullivan (2013), who modeled covariances of turbulently fluctuating clear-air radar reflectivity and the turbulently fluctuating radial wind velocity. They found that such covariances can lead to Doppler velocity biases similar to those observed with vertically pointing wind profiling radars operating in this region. It is likely that this is a viable mechanism for the vertical velocity biases generally observed by atmospheric radars throughout the atmosphere.

An extension of the TDI analysis for wider beam DBS radars to correct for uncertainties in the actual beam direction, called HDI, was applied by Holdsworth and Reid (2004a) at MF and by Reid et al. (2005) at VHF. In HDI, the transmitter beams are formed and directed as for normal DBS radars, but the effective pointing angle of the receiver beam is formed and measured interferometrically. Post statistics beam steering (PSS) (e.g., Kudeki and Woodman 1990) is used to form a receive beam which is steered through a grid of beam directions. The power for each beam direction is determined, and the effective beam position (EBP) is found by applying a 2-D Gaussian to estimate the direction of maximum power. The receive beam is then re-steered in the direction of the EBP, and the standard DBS parameters are estimated. The term “hybrid Doppler interferometry” is used as the technique is a hybrid of Doppler and interferometric techniques. Holdsworth and Reid (2004a) also used in HDI preference to time domain interferometry, since the analysis can be applied in either the time or frequency domain.



The use of PSS allows the EBP to be determined more accurately (and to lower SNRs) than using the mean angle of arrival (MAOA), since it uses combined receiver outputs, while the MAOA is estimated by cross-correlating single receiver outputs. The technique can also be usefully applied to wider vertically directed transmitter beams to determine the mean angle of arrival. The ability to determine the actual beam form is clearly an advantage, and the technique appears to work well.

With sufficient spread in the angles of arrival of the measured radial velocities in the TDI technique, it is also possible to measure the horizontal wind components. Thorsen et al. (1997) provided a more extensive theoretical formulation for the TDI approach and considered ordinary and total least squares fitting to TDI radial velocities to derive the mean and fluctuating components of the wind field. In so doing, they extended TDI to measurements of the three-dimensional mean winds and of the Reynolds stress tensor for small MF/HF PR SA radars. In this, they anticipated a similar approach applied by Hocking (2005) to derive the same parameters from all-sky meteor radars. Thorsen et al. provided promising results from the Urbana MF radar, but their insightful approach has not been further investigated.

However, preliminary investigation of the application of HDI to the BPMF radar indicates good results and suggests that it should perhaps be applied in preference to hardware beam forming when using this radar because of the effects of aspect sensitivity on the relatively wide polar diagram of the antenna array (Spargo et al. 2015). How well horizontal velocities can be measured in the wide vertically directed beams of small MF/HF PR SA radars depends on the aspect sensitivity of the backscatter, and as we have seen, this is very high at heights below about 80 km. This may restrict the application of the technique to height ranges where more isotropic backscatter is typical.

By way of example, Fig. 18 shows the mean angles of arrival determined using the HDI technique for a 13 day observational period using the BPMF radar in 1998. For these observations, the radar transmitter beam was successively steered between five beam positions. These were 12° off-zenith towards the east, west, north, south, and vertical, and so a cycle took 10 min to complete. The transmitter beam 3 dB contours are shown in the figure. Reception was on 16 receivers. Inspection of this diagram indicates the effect of the aspect sensitivity on the effective beam position for each 2 min observation and the great variability in the actual angle of arrival over time.

Figure 19 shows an example of the mean density normalized upward flux of zonal ( $\langle u'w' \rangle$ ) and meridional ( $\langle v'w' \rangle$ ) momentum measured over a 6 day period using the same configuration as shown in Fig. 18, but

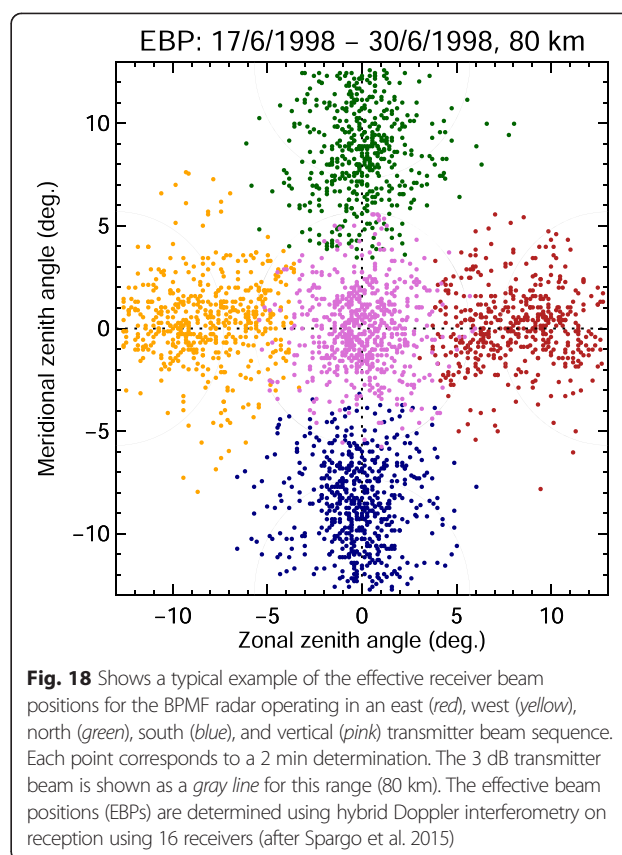


**Fig. 18** Shows a typical example of the effective receiver beam positions for the BPMF radar operating in an east (red), west (yellow), north (green), south (blue), and vertical (pink) transmitter beam sequence. Each point corresponds to a 2 min determination. The 3 dB transmitter beam is shown as a gray line for this range (80 km). The effective beam positions (EBPs) are determined using hybrid Doppler interferometry on reception using 16 receivers (after Spargo et al. 2015)

with an off-zenith angle of 13°. To calculate these terms, three approaches were used. In the first, the mean aspect sensitivity was calculated and used to correct the apparent beam direction and the density normalized Reynolds stress terms ( $\overline{u'^2}$ ,  $\overline{v'^2}$ ,  $\overline{w'^2}$ ,  $\overline{u'w'}$ ,  $\overline{v'w'}$ ,  $\overline{u'v'}$ ) were calculated using the approach of Vincent and Reid (1983) by fitting to all five beams. This results for this approach for the  $\overline{u'w'}$  and  $\overline{v'w'}$  terms are shown as the red line. The second approach calculated the density normalized Reynolds stress tensor by taking the radial velocities corresponding to the angle of arrivals and performing a least squares fit to these to obtain the six Reynolds stress terms. The results are shown as the black line. The last analysis used this same approach but only used the angles of arrival from the vertically directed beam. This resulted in this observation being made over only 20 % of the observation time for the red and black profiles. This is shown as the gray line in Fig. 19.

Inspection of this diagram indicates good agreement in form between the red and black height profiles. While noisier, the gray profile looks similar in form. Note that this last analysis is a version of that suggested by Thorsen et al. (1997) and for this case, with a relatively narrow transmitter beam (~20° for these observations), appears to deliver a tolerable result for this difficult to measure



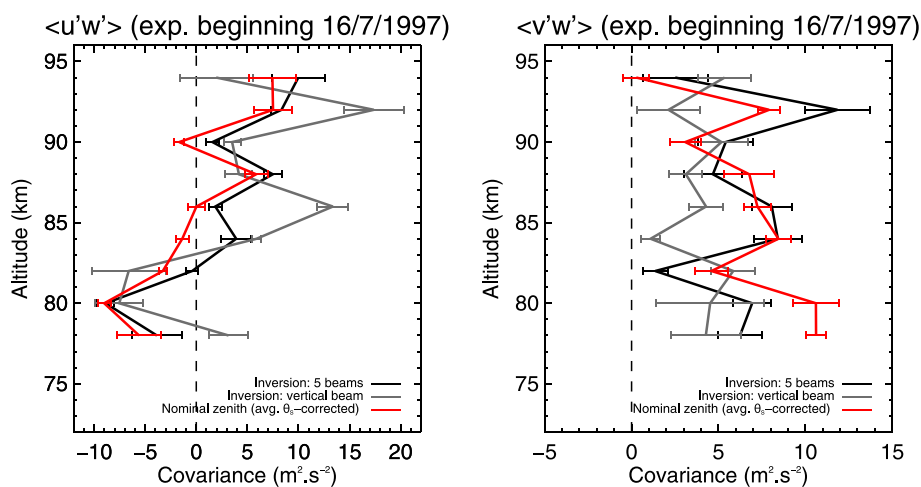


**Fig. 19** The mean upward flux of horizontal momentum for the zonal (*left*) and meridional (*right*) directions for a 5 day period in July 1997 using the five beam arrangement shown in Fig. 18. The *red line* indicates these terms calculated by using the Vincent and Reid (1983) approach with the five nominal beam directions after correcting them for the aspect sensitivity of the atmosphere. The *black line* uses the radial velocities corresponding to each of the calculated 2 min effective beam positions and calculates the Reynolds stress tensor from these. The results indicated by the *gray line* are calculated in the same way as the *black line* but using only the vertically directed beam. These then correspond to the Thorsen et al. (1997) approach described in the text (after Spargo et al. 2015). For further details, see the text

parameter. This is a preliminary result but suggests some hope of measuring these terms with small MF/HF PR radar systems.

#### Lataitis slope technique

Other analysis approaches to SA data are described by Lataitis et al. (1995), Doviak et al. (1996), and Holloway et al. (1997). Lataitis et al. (1995) showed that the slope of the cross-correlation amplitude at zero lag, normalized by the level of the cross-correlation amplitude at zero lag, is directly proportional to the component of the wind velocity along the antenna pair baseline. Using this approach and three non-collinear antenna locations, they were able to determine the wind velocity. They found that their “slope technique” was sensitive to the degree of vertical anisotropy of the scattering medium and suggested that it was best suited to the situation of scattering from isotropic to moderately anisotropic turbulence. This would correspond to wind profiling in the atmospheric boundary layer. Doviak et al. (1996) and Holloway et al. (1997) further considered the application of spaced antenna technique in situations of more isotropic turbulence, a condition more likely to hold only as generally true in the troposphere when using upper VHF, UHF, or higher frequencies. For example, in a typical study, Tsuda et al. (1997) found significant aspect sensitivity at lower VHF in the troposphere and lower stratosphere when using the MU radar in Japan.

More recent work has considered the application of the technique to UHF boundary layer radar (Cohn et al. 2001), and to weather radar (e.g., Zhang and Doviak 2007; Venkatesh and Frasier 2013), and has

revisited the theoretical formulation of the analysis. Venkatesh and Frasier (2013) provide a good brief contemporary review of SA analysis techniques.

#### Doppler beam swinging

Traditional Doppler beam steering radar, in which transmitter and receiving beams are formed and used to measure radial velocities in a number of look directions, is rare at MF and lower HF because of the physically large array size needed to obtain the relatively narrow beams needed for the technique at these wavelengths. In DBS, beams may be formed in hardware or software, but we use the DBS term to apply where there is no further interferometric correction to determine the actual angle of arrival of the returned signal. There are only three MF/HF radars currently capable of operating in this mode. These are the BPFM large array (Briggs et al. 1969; Reid 1987; Reid 1988; Reid et al. 1995; Holdsworth and Reid 2004a), the large Saura HF crossed array radar (Singer et al. 2003, 2008, 2011), and the smaller Juliusruh crossed array HF radar. The BPFM uses a filled array as shown in Fig. 6, while the Saura HF radar uses a cross type antenna array as shown in Fig. 3. A large MF/HF cross type antenna array on Bribie Island in Australia used a sophisticated raster style of operation to image the ionosphere at three different frequencies (see e.g., Lingard 1996a,b) until retired in the 1990s, and is particularly noteworthy as a precursor to the Saura HF radar (Singer et al. 2008), and to crossed type partially filled radars generally (Hocking and Thayapaxan 1997).

A very important point here is that the complex data received on any one receiver has the same form

for FCA, FSA, SCA, IDI, HDI, TDI, or Doppler beam steering, but the analysis applied differs. The Doppler beam swinging and spaced antenna methods use the same information. The DBS technique exploits the change in the mean Doppler shift with azimuth angle and samples small spatially separated volumes. The SA correlation methods make use of the fact that the variation in the Doppler shift with angle is such that the resultant field moves over the ground as a random pattern with a velocity twice that of the horizontal wind at the backscatter height. Briggs (1980) provides a complete discussion.

We illustrate the idealized situation in Fig. 20 which is adapted from Briggs (1980). In this figure, the atmosphere at height  $z$  is moving with a horizontal velocity  $u$ , so that the electric fields from paths 1 and 2,  $E_1$  and  $E_2$ , are given by

$$E_1 = E_0 \exp\left\{i\left[\omega_0\left(1 + \frac{2u}{c}\sin\theta\right)t - \frac{2\pi x \sin\theta}{\lambda} + \frac{2\pi z \cos\theta}{\lambda}\right]\right\},$$

and

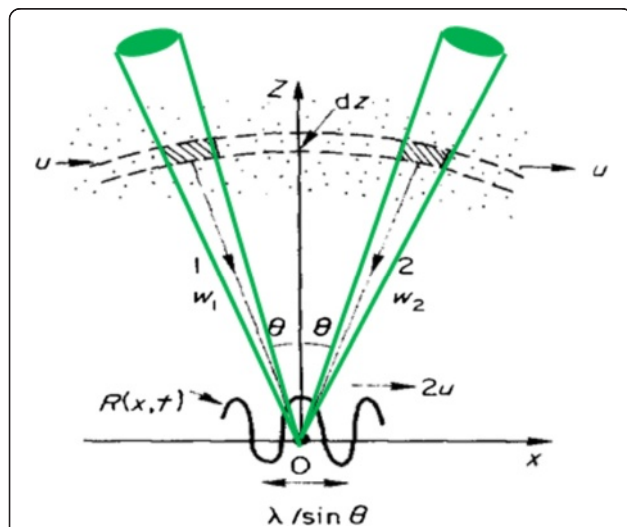


**Fig. 20** (Modified from Briggs 1980). The situation described in the text outlining the basis of the formation of the ground diffraction pattern in the SA experiment. Here, the electric fields produced by volume scatter from a moving atmosphere at angles of  $\pm\theta$  sum to produce an electric field on the ground, the real part of which is a sinusoid of wavelength  $\lambda/\sin\theta$  that moves with twice the velocity of the atmosphere at the backscatter height. When a broad range of angles is illuminated, the sinusoids from each pair of angles sum to produce the moving ground diffraction pattern. DBS techniques use a narrower angular range of angles (such as those outlined in green) to measure the line of sight Doppler shift. When these are obtained from a number of angles and statistical homogeneity of the wind field is assumed, the three-dimensional wind field can be reconstructed. Interferometric techniques use Doppler shifts associated with randomly distributed scattering centers to determine a mean velocity

$$E_2 = E_0 \exp\left\{i\left[\omega_0\left(1 - \frac{2u}{c}\sin\theta\right)t + \frac{2\pi x \sin\theta}{\lambda} + \frac{2\pi z \cos\theta}{\lambda}\right]\right\},$$

at the ground. Here  $\omega_0$  is the radar angular frequency, and  $\omega_1$  and  $\omega_2$  are the Doppler shifted radar frequencies given by

$$\omega_1 = \omega_0 + 2\omega_0\left(\frac{u}{c}\right)\sin\theta,$$

and

$$\omega_2 = \omega_0 - 2\omega_0\left(\frac{u}{c}\right)\sin\theta,$$

and the other terms have their usual meanings. The real part of the sum of the electric fields at the ground produces a sinusoidal variation in electric field strength on the ground with a wavelength  $\lambda/\sin\theta$  that moves with a velocity  $2u$  and is given by

$$R(x) = 2E_0 \cos\left(\frac{2\pi \sin\theta}{\lambda}x - \frac{2\omega_0 u t \sin\theta}{c}\right).$$

Each pair of angles  $\pm\theta$  produces a particular sinusoid, and these all sum to produce the moving ground diffraction pattern. Smaller spatial scales in the diffraction pattern are produced by returns from larger off-zenith angles, and so the effect of using groups of antennas on reception is to filter out higher frequency spatial scales. Of course, this just corresponds to using a narrower polar diagram on reception. In the SA experiment, the antenna spacing is selected so that the cross-correlation functions between antenna pairs have values of around 0.5 on average. This varies with height (see Fig. 8), and so in this sense, the experiment is optimized for a particular height or range of heights. This can be thought of as being somewhat analogous to selecting a particular off-zenith angle in the DBS experiment.

Note that a differential vertical velocity, that is, one which is not the same in beams 1 and 2 will produce an apparent motion of the ground diffraction pattern. A similar effect occurs in the DBS technique, and as we discuss in the section on meteor radars below, this may limit the minimum time resolution available for measuring winds in all of these techniques. Generally, an averaging time of about 1 h is considered reliable.

DBS techniques use a narrower angular range to measure the line of sight Doppler shift, and when these are obtained from a number of angles, and statistical homogeneity of the wind field is assumed, the three-dimensional wind field can be reconstructed (e.g., Reid 1987). Interferometric techniques use Doppler shifts associated with randomly distributed scattering centers to determine a mean velocity. In this, they are similar to all-sky meteor radar techniques (Holdsworth et al. 2004a). The hybrid Doppler interferometer combines relatively narrow

transmitter beams with interferometric reception, and so, we have described it in the SA section above.

Great care must be taken when using DBS at MF and HF because of the high aspect sensitivity of the MLT region at these frequencies (see e.g., Reid 1988) and the relatively wide beams available. This results in the effective beam pointing angle being less than the apparent beam angle (e.g., Reid 1988; Vandeppeer and Reid 1995b; Holdsworth and Reid 2004a). This can be corrected by using HDI as noted above, but this is a further limitation for MF and lower HF radars even when it is possible to build arrays large enough for DBS.

#### ***MF/HF radar: strengths and weaknesses***

As we have seen, the strengths of the MF/HF SA technique include moderate range and good time resolution, with values of 2 to 4 km height resolution and 2 to 5 min time resolution for wind measurements being typical. The height coverage is good, with typical values from 60 to 98 km during the day and 80 to 98 km during the night (see Figs. 13 and 14). The upper usable height depends on the total reflection height and also on the ability of the data acquisition system to cope with the very large dynamic range in echo strength in the 60 to 100 km height range. We will return to this point below. MF radars operate with high peak powers, but very low average powers and duty cycles (typically less than 0.5 %). Power consumption is low, and reliable continuous long-term operation has been demonstrated consistently at a number of locations; for example, the Saskatoon MF SA radar has operated continuously since 1979, and the Adelaide MF SA radar continuously since 1984.

The limitations of the techniques include a degradation in height resolution through range smearing if the angular scatter is wide (with a half-power half-width greater than about 10°). This is because the actual beam pattern is the product of the antenna polar diagram and the polar diagram of the backscattering irregularities. The simple antennas used in the spaced antenna technique have wide angular polar diagrams, and so, this product also produces a wide effective beam when the backscatter angular polar diagram is wide.

The large increase in the returned echo power as illustrated in Figs. 4 and 11 requires a large dynamic range within the receiving and data acquisition system, and a variety of approaches have been utilized. These have included a three-step variable gain system with height used with the Saskatoon MF radar (Meek 1979) and alternate low- and high-mode gains for the 60 to 80 and 80 to 100 km height ranges, respectively, and an adaptive gain system (e.g., Vandeppeer and Reid 1995b). This was a particular issue for older systems with limited digitization. Most current systems now use 12-bit or larger digitization

schemes and so have corresponding larger dynamic ranges.

The rapid increase in power with height typical at MF and lower HF for the MLT region has restricted the application of pulse coding techniques at these frequencies. However, this could have considerable utility in the 40 to 80 km height region with 4 bit and 8 bit codes and 1 km bit lengths.

Czechowsky et al. (1983) do report on an intriguing radar backscatter experiment at 2.75 MHz using a peak power of 1.2 MW and a maximum duty cycle of 4 %. Their experiment was conducted at Tromsø using the heating facility transmitter in winter and used “limited pulse coding”. With this very high peak power, they reported finding echoes from 15 to 35 and from 52 to 100 km during their brief experiment. Belrose (1970) does report the ability to measure electron densities in the 40 to 80 km height region during times of abnormally high ionization, and Holdsworth and Reid (1997) report measurements from 52 km upwards, so there is some additional evidence to support their observations.

The Czechowsky et al. result for echoes below 40 km does not appear to have been replicated since, and there are potential complications because of range aliasing, but the results are interesting enough to justify repeating the experiment. This could be done in the region above 30 km using a (typically available) 64 kW transmitter, large antenna array, and an 8 bit code with 1 km bit length. This would lead to a power aperture (PA) product smaller than that of Czechowsky et al.’s (1983) experiment but would allow much longer observation times and a more systematic investigation of the possible appearance of stratospheric echoes at MF. However, it is noteworthy that stratospheric echoes have not been reported by the Saura HF radar at a similar latitude and location to Czechowsky et al.’s observations.

Simple 2 bit pulse coding may also be useful in discriminating out interfering signals, which is sometimes an issue at MF and HF, and this has been implemented on the Saura radar to reduce interference from HF communications (Mayo 2015).

Finally, relatively large land areas are required for the simple antennas used in the SA technique, although it is possible to share the land with cropping or other agricultural activities as is done with the Indian MF radars.

#### ***Investigation of the IDI and FCA analysis applied to MF and HF radar techniques***

The MF/HF SA technique has been somewhat controversial as a technique when applied to measuring MLT winds. This has resulted from its evolution from its original application to total reflection from the ionosphere, and the elementary analyses applied to the original experiments, largely because of computational limitations.

These original measurements are certainly problematic. This was further compounded by the evolution of the acceptance criteria that were applied to constrain the data, the uneven adoption of both these quality control measures and the more sophisticated analyses such as the FCA, which took account of the real nature of the ground diffraction pattern, and a lack of care in excluding backscatter contaminated by total reflections above about 92 to 94 km at some times and locations. The current FCA includes 18 QC measures (see Table 6) that have often, but not exclusively, evolved based on experience in applying the analysis, rather than from derivations from first principles.

In the 1990s, considerable useful investigation of MF/HF SA radar techniques occurred. This was because of a number of factors, which we now discuss and which are still relevant and instructive, because some of the results were over generalized and not necessarily critically assessed subsequently.

#### ***AIDA 89 campaign***

The first of these was the AIDA 89 campaign during which very mixed quality results were obtained above 80 km when an HF radar using the simple IDI analysis was compared to other techniques (Hines et al. 1993). Hines argued that this was a result of gravity wave contamination of the measured IDI winds resulting in the phase velocities of the gravity waves being measured instead of the actual background wind and generalized this argument to all MF/HF SA radars. This particular argument had previously been used for MF/HF SA radars using total reflections from the ionosphere and the similar fades technique, where it could be valid (see e.g., Hines and Rhagava Rao 1968). However, it is not valid in the case of partial reflections (see e.g., Hocking et al. 1989), and in any case, gravity wave effects, if any, would be the same as those experienced by all atmospheric radars operating at frequencies up into the VHF band. Hines subsequently agreed that this would be the case (private communication, 1994), but it is not observed at MF, or any other frequency.

The Hines et al. (1993) results motivated experimental (Vandepier and Reid 1995a), theoretical (Briggs 1995), and modeling (Holdsworth and Reid 1995a,b) investigations of the IDI analysis. These found that the simplest IDI analysis produced results similar to the apparent velocity of the FCA, and that the presence of (apparent) discrete scattering centers was inevitable even in the case of volume scattering. The Holdsworth and Reid (1995a) model used point scatterers, which would correspond to a volume scatter situation, but included aspect sensitivity in the radar scattering volume, so that the anisotropy of the real atmosphere was accounted for.

The Hines et al. (1993) results also motivated modeling studies by Kudeki et al. (1993) and Surucu et al. (1995). These studies suggested that MF/HF SA wind measurements were suitable for measurement periods longer than about 1 h. Hocking (1987) noted that wind measurements made over shorter time intervals were potentially usable, but some care needed to be exercised to recognize the potential contaminating effects of vertical velocities associated with short period gravity waves on the results. In this, the SA techniques are no different to DBS (e.g., Reid 1987) or all-sky meteor radar techniques (see below).

Turek et al. (1995) revisited the Hines et al. (1993) AIDA IDI intercomparisons, included many more observations, and re-analyzed the IDI data using the Saskatoon and Adelaide implementations of the FCA. They found much better agreement between the various techniques, but they did find that the relationship between the true and apparent FCA velocities, and the interferometric velocities remained to be clarified. We have discussed this above, and as we noted there, subsequent detailed investigation by Holdsworth and Reid (2004b) found the IDI technique valid when relatively narrow beams were used and careful selection criteria were applied. They also concluded that with these improvements, the technique had some real advantages over the FCA. The numerical modeling work of Holdsworth and Reid (1995b, 1997) failed to find any evidence of the gravity wave contamination effects proposed by Hines et al. (1993) in the IDI. Holdsworth and Reid (1997) also investigated the FCA analysis in some detail using their model and confirmed that the gravity wave arguments of Hines were not valid for this analysis either.

From these investigations, it was clear that the AIDA 89 IDI results reported by (Hines et al. 1993) were not at all typical of modern MF/HF SA radars in general or of analyses that were more sophisticated than the similar fades analysis that was current in the 1960s. The subsequent investigations showed that although the FCA technique did underestimate the wind magnitude, it was a valid method of measuring winds in the MLT region, particularly for periods longer than about 1 h. The investigation of the IDI and FCA analyses is discussed in some detail by Reid (1996) and Holdsworth and Reid (2004b).

#### ***Interferometric techniques***

The second reason for the close scrutiny of MF/HF SA techniques was the development of a new radar interferometric techniques and their application at MF (e.g., Meek et al. 1986a, 1986b). This was facilitated by the use of better hardware using coherent receiver systems, but more importantly, as we have noted above, more powerful affordable computers. This development in



itself was an exciting evolution, but the technique we have discussed at some length, IDI, was offered as an MF/HF SA radar technique analysis not subject to the limitations or doubts of the FCA analysis.

However, as noted above, the simplest IDI analysis measures the apparent velocity. More sophisticated IDI analyses do not necessarily have an advantage over the FCA when applied to the standard SA configuration, which has relatively wide beams, and additional care must be taken with system phase calibration. However, again as noted above, it does have advantages in the case of narrower beam radars (Holdsworth and Reid 2004b), and importantly, it does allow some other MF/HF radar types to measure MLT winds. For example, the dynasonde (see e.g., Rietveld et al. 2008) for a description of a modern dynasonde at Halley was configured to operate in an IDI mode (Jones et al. 1997) and was successfully used to measure MLT winds prior to being relocated in 2008. Other dynasondes, such as that at Bear Lake in Utah, have since been successfully used in similar ways (Jones et al. 2003). These radars are included in Fig. 1 and Table 3.

#### **Satellite intercomparisons**

The third reason for intercomparisons was that satellite-derived MLT winds became generally available for the first time with the launch of the Upper Atmosphere Research Satellite (UARS) satellite and the high resolution Doppler interferometer (HRDI) and Wind Imaging Doppler Interferometer (WINDII) instruments it carried (e.g., Reber et al. 1993). These instruments provided a powerful global view of the wind field of the planet. In addition to studying MLT region atmospheric dynamics, they also provided the means and motivation for the intercomparison of MLT winds derived from different techniques for the purposes of ground proofing the satellite measurements (e.g., Palo et al. 1997), and provided a better understanding of the limitations of the various measurement techniques.

Intercomparisons between HRDI and a number of MF/HF SA FCA radars found that mean and tidal component winds in the satellite instrument were larger than the corresponding radar winds (e.g., Khattatov et al. 1996), and Burrage et al. (1996) concluded that HRDI measured larger winds than MF radars, but that the size of the difference varied from radar to radar. Burrage et al. (1996) concluded that the HRDI results were more consistent with falling sphere measurements and with WINDII measurements and so by inference that MF wind magnitudes were too small. It is worth noting that the HRDI measurements represented averages over several hundred kilometers in the meridional direction. This was certainly recognized in the HRDI results referenced above, where the importance of differences in time and

space averaging, the short-term variability of tides, mean winds, and other motions, and the presence of non-migrating tides and other longitudinal irregularities on the intercomparison were noted. However, as we have seen elsewhere in this review, the most likely, and probably the dominant reason for the discrepancy between the satellite and MF radar results, was the underestimation of the wind magnitude in the SA FCA analysis.

#### **Rebirth of the meteor radar technique for measuring MLT winds**

The last reason for these intercomparisons was the re-development of meteor radars for measuring MLT region winds and the consequent comparison with the MF/HF SA FCA radar winds. This started with the application of narrow beam VHF stratospheric tropospheric (ST) radars to meteor studies (e.g., Valentic et al. 1996; Elford 2001) and followed with the development of purpose-built, compact, all-sky VHF meteor radars (e.g., Hocking et al. 2001; Holdsworth et al. 2004a). For example, in the first of these intercomparisons, Cervera and Reid (1995) found an underestimation of the MF/HF SA FCA winds in the 80 to 100 km height region when the Adelaide BPFM radar winds were compared to meteor winds measured using the collocated Adelaide narrow beam VHF ST radar operating in meteor mode. The underestimation varied with height, but FCA wind magnitudes were typically between 0.6 and 0.8 of the meteor wind magnitudes. This and the many comparisons that followed (e.g., Thayaparan and Hocking 2002) demonstrated that MF/HF SA FCA winds were an underestimate of the actual wind magnitude, but that their directions were correct.

As we have noted elsewhere in this review, other MF/HF SA analysis techniques, including IDI and the SCA do not appear to be as susceptible to this underestimation, although larger antenna arrays would be required to fully realize this advantage. MF meteor radars are also not subject to this underestimation but are limited in other ways.

#### **MF/HF meteor radars**

Meteor radars operating near 30 MHz in the HF and lower VHF bands are not subject to an upper useable height governed by total reflection but rather from the upper detectable height for meteor trails (e.g., Greenhow and Hall 1960). At these frequencies, the number of meteor detections tends to zero near 110 km. Generally, the lower the operating frequency, the greater the maximum useable height, so that for example at 2 MHz, meteor trails are detected to heights near 120 km (e.g., Steel and Elford 1991; Tsutsumi et al. 1999). However, as we have noted above, the drift and diffusion of meteor trails is increasingly affected by the Earth's magnetic field above 110 km and measuring parameters related to the neutral

atmosphere requires some care. Nevertheless, Holdsworth and Reid (2004a) report nighttime winds to 120 km with the BPME, and Tsutsumi and Aso (2005) report regular wind measurements to 120 km during geomagnetically quiet conditions at high latitudes using the Syowa MF radar (69°S). However, the routine use of MF radars as meteor radars is unlikely to be practical, and this application is most likely restricted to special observations at suitable locations.

One issue with all-sky meteor radars relates to the distribution of the radial velocities measured across their wide observing areas. This is never uniform, and varies significantly with time of day, through the year, and with latitude. Using a simple model, Reid (1987) demonstrated the limitations of Doppler radars with different beam geometries in measuring atmospheric parameters. Kudeki et al. (1993) also considered the impact of inhomogeneous winds fields on SA, DBS, and IDI radar measurements using theoretical arguments and concluded that such inhomogeneity could lead to significant biases in such measurements. Surucu et al. (1995) extended the Kudeki et al. (1993) model to include both isotropic and non-isotropic scatterers and concluded that the SA radars produced the horizontal wind as long as any waves present had horizontal scales larger than the horizontal scale of the SA radar pulse volume. Hocking (1987) concluded that these effects would not be of concern for MF/HF SA wind measurements of periods longer than an hour or so.

If meteor radars are considered as Doppler radars with randomly varying beam directions, then it would not be too surprising to find that they are also subject to limitations in just what parameters that they can measure with reasonable uncertainties. More sophisticated modeling using gravity wave fields of meteor radar observations by Spargo et al. (2015) has shown similar limitation for meteor radars to those found for DBS radars by Reid (1987).

Nevertheless, modern meteor radars are powerful instruments, capable of measuring the horizontal winds for periods longer than about an hour, the radiants of meteor showers (Jones and Jones, 2006), the speed of the meteoroids (Holdsworth et al. 2007), the density of the neutral atmosphere (Younger et al. 2015), and its temperature in some instances (Holdsworth et al. 2006; Younger et al. 2014). The extension of these developments to meteor radars operating in the HF band would be significant, and Chisham and Freeman (2013) review the potential of SuperDARN radars as meteor radars. Generally, SuperDARN radars lack the optimized interferometric capability of all-sky meteor radars (e.g., Holdsworth et al. 2004a), and this limits their capability somewhat. However, consideration of the expected count rate using McKinley's (1951) relation suggests meteor counts with a typical SuperDARN configuration

would be around 40,000 per day at the typical SuperDARN operating frequency of 12 MHz. This would be a significant extension of the capability of these HF band radars and a significant addition to our understanding of the dynamics of the MLT region.

#### ***Differential absorption experiment/differential phase experiment***

The DAE proposed by Gardner and Pawsey (1953) estimates the electron density using the amplitude ratio of the extraordinary to ordinary mode signals returned from the ionospheric D region. The application of this technique was an active area of research until the early 1980s (see e.g., Belrose 1970; von Biel 1977; Manson and Meek 1984). The technique provides a coarse measure of the electron density, but relative changes in electron density can be closely monitored.

After not being utilized for some years, the DAE and DPE were applied to new MF/HF radars that began being produced in the early 2000s onwards (see, e.g., Holdsworth et al. 2002; Vuthaluru et al. 2002; Singer et al. 2003). They are now routinely applied on many MF/HF radars, with the most sophisticated results perhaps being obtained on the Saura radar in northern Norway (e.g., Singer et al. 2008, 2011). Figure 4 shows power profiles for both O and X modes, as well as the electron densities calculated using both the DAE and DPE. Figure 21 shows an intercomparison from the Saura radar operating in DAE/DPE mode with results from a rocket borne Faraday rotation and absorption experiment (Singer et al. 2011). These authors also show a number of other intercomparisons that demonstrate the utility of the technique. The DAE and DPE techniques also allow the collision frequencies to be derived (Vuthaluru et al. 2002), and these are directly related to pressure, suggesting that this parameter might also be able to be recovered from the experiment.

#### **Conclusions**

MF/HF partial reflection radars remain one of the few techniques available to routinely measure winds in the 55 to 80 km height region. They also offer the ability to measure winds in the 80 to 92 km height region, as well as turbulent velocities, and D region electron densities. However, the detailed nature of the irregularities in the 50 to 90 km height region is still not understood nor is the underlying reason for the occurrence of preferred heights of echo occurrence. This lack of understanding limits the ability to clearly interpret some aspects of the measurements from these radars. The clustering of instruments, ideally including high powered LIDARs, offers the opportunity to resolve some of these uncertainties.

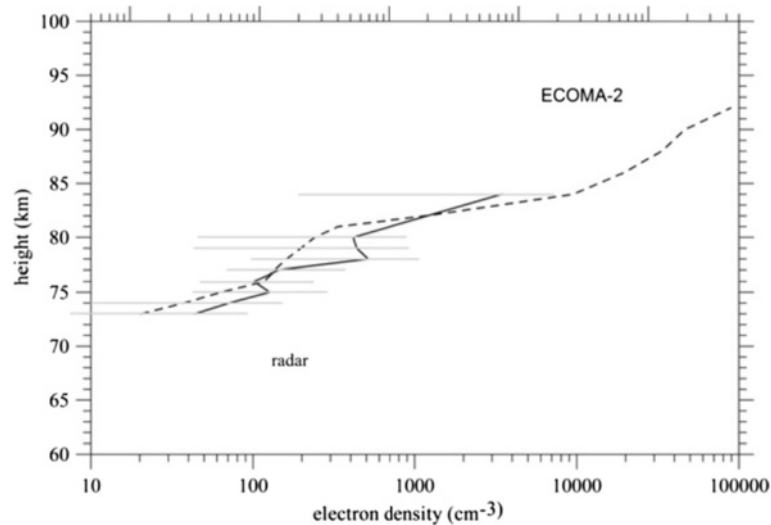


**Fig. 21** Electron density profiles by DAE/DPE measurements (full lines, 20:50–21:20 UT, solar zenith angle 106°) and electron density profiles from the in situ radio wave propagation measurements (dashed lines) of the ECOMA-2 flight on September 17, 2006, 21:06 UT. The error bars represent the quartile limits (after Singer et al. 2011)

Uncertainty about the reliability of the technique and the availability of all sky meteor radars has led to some decline in its popularity. However, the technique is robust and offers a variety of analysis possibilities. The FCA is the most commonly applied analysis, its major deficiency being an underestimation of 15 to 40 % of the wind magnitude at MF/HF, but not its direction, for an ideally configured small system. This is unacceptably high for studies of dynamics. For comparison, typical values for small VHF SA systems may be closer to between 5 and 10 % and not obviously height dependent. For MF/HF SA radars running the FCA, there is a strong height dependence in the bias. The reason for this remains to be investigated, but inadequate sampling of the ground diffraction pattern may be an explanation. The use of sampling schemes optimized for the characteristics of the fading time series is recommended. Such a scheme would ideally be dynamic, so that it would potentially be different for each sampled height and vary with time.

The SCA, IDI, TDI, and HDI techniques offer additional possibilities for measuring MLT winds when appropriate acceptance criteria are applied to the data, and in the case of IDI, TDI, and HDI, when narrower transmitter beams are available, and when this is done, the underestimation bias characteristic of the FCA is not evident. Importantly, all SA systems should correct for receiver channel phase differences.

Care needs to be taken with winds measured above about 92 km with all MF/HF radar systems particularly near mid-day because the dominance of the E region total reflection and the potential for group retardation. We recommend using the best possible practical height

resolution and utilizing the calculated total reflection heights to omit contaminated data. We also recommend the implementation of additional QC measures to detect and omit data contaminated by total reflections.

Based on experience at VHF, correction of the known bias in wind magnitude in the FCA should be possible and, if so, should be applied. One issue in this context is a general lack of techniques for intercomparison below about 80 km. The question of whether MF/HF SA wind fields should be quality controlled is still open, but we would recommend its adoption. The application of more sophisticated experimental techniques such as pulse coding to improve the height coverage at lower heights, improve range resolution, improve duty cycles, and reduce interference is suggested, as are the introduction of range imaging (RIM)-like techniques (e.g., Yu and Palmer 2001), and further exploitation of MF meteor echoes. These developments will continue to extend the technique, as will hardware improvements, which are continuing generally with atmospheric radar.

Long MF/HF SA FCA data sets exist, and in spite of the known underestimation in wind magnitude, investigation of long-term changes in the MLT wind field is providing promising results (e.g., Hoffmann et al. 2011). With very similar MF/HF SA and meteor systems now operating, the idea of a “ground based satellite” and the development of virtual observatories has great appeal. This is being pursued through a number of projects, including the Madrigal database (<http://madrigal.haystack.mit.edu/madrigal/>) and IUGONET global observation network (<http://www.iugonet.org/en/>). The availability of relatively inexpensive radars with complementary attributes such as MF/HF partial reflection radars and

all-sky meteor radars with global geographical spread, combined with a global assimilation system will greatly facilitate our understanding of the MLT, and this is the likely future of these systems. This is certainly the case for the East Asia Oceania region shown in Fig. 1.

## Additional files

**Additional file 1: The amplitude only variation of radio waves received at one antenna on the BPMF radar in the 1970s.** (WMV 2364 kb)

**Additional file 2: The time variation of the ground diffraction pattern at 2 MHz for a partial reflection height of 80 km. This is taken from movies produced by Briggs and Holmes (1973) and Holmes (1975) and described by Briggs (1993).** (WMV 560 kb)

## Abbreviations

AIDA: Arecibo Initiative Dynamics of the Atmosphere; AM: amplitude modulation; BLT: boundary layer troposphere; BPMF: Buckland Park medium frequency radar; BPVHF: Buckland Park very high frequency radar; CCF: cross-correlation function; DAE: differential absorption experiment; DBS: Doppler beam swinging; DPE: differential phase experiment; E-Mode or X-mode: extraordinary mode; FCA: full correlation analysis; FSA: full spectral analysis; HDI: hybrid Doppler interferometry; HF: high frequency; HRDI: high-resolution Doppler interferometer; IDI: imaging Doppler interferometry; LIDAR: laser radar; MAOA: mean angle of arrival; MF: medium frequency; MLT: mesosphere lower thermosphere; MST: mesosphere stratosphere troposphere; O mode: ordinary mode; PR: partial reflection; PRF: pulse repetition frequency; PRP: pulse repetition period; RADAR: radio detection and ranging; RIM: range imaging; SCA: spatial correlation analysis; SNR: signal to noise ratio; ST: stratospheric tropospheric; SuperDARN: super dual auroral radar network; TDI: time domain interferometry; TSE: triangle size effect; UARS: Upper Atmosphere Research Satellite; UHF: ultrahigh frequency; VHF: very high frequency; VLF: very low frequency; WINDII: Wind Imaging Doppler Interferometer.

## Competing interests

The author declares that he has no competing interests.

## Author's information

IMR is a Professor of Physics at the University of Adelaide and the Executive Director of the ATRAD group of companies.

## Acknowledgements

IMR gratefully acknowledges Andrew Spargo, Bronwyn Dolman, Bob Vincent, and Andrew MacKinnon for reading early drafts the manuscript and Andrew Spargo for assistance in preparation of some of the figures.

Received: 23 February 2015 Accepted: 14 September 2015

Published online: 19 October 2015

## References

- Abdu MA, Ananthakrishnan S, Krishnan BA, Massambani O (1973) Cosmic ray ionization in the D region at sunrise: evidence from VLF phase measurements. *Radio Sci* 8(8-9):733-6, <http://dx.doi.org/10.1029/RS008i008p00733>
- Adams W, Brosnahan JW, Walden DC, Nerney SF (1986) Mesospheric observations using a 2.66-MHz radar as an imaging Doppler interferometer: description and first results. *J Geophys Res* 91:1671-83, <http://dx.doi.org/10.1029/JA091iA02p01671>
- Andrews DG, Holton JR, Leovy CB (1987) Middle atmosphere dynamics. Academic, San Diego, California, p 489
- Appleton EV (1930) On some measurements of the equivalent height of the atmospheric ionized layer. *Proc Roy Soc A* 126:542-69, <http://dx.doi.org/10.1098/rspa.1930.0025>
- Appleton EV, Barnett MAF (1925) Local reflection of wireless waves from the upper atmosphere. *Nature* 115:333-4, <http://dx.doi.org/10.1038/115333a0>
- Appleton EV, Piddington JH (1938) The reflection coefficients of ionospheric regions. *Proc Roy Soc A* 164:467-76, <http://dx.doi.org/10.1098/rspa.1938.0031>
- Bailey DK, Bateman R, Kirby RC (1955) Radio transmission at VHF by scattering and other processes in the lower ionosphere. *Proc IRE* 43:1181-231, <http://dx.doi.org/10.1109/JRPROC.1955.277933>
- Bain WC, May BR (1967) D-region electron density distributions from propagation data. *Proc IEE* 114:1593, <http://dx.doi.org/10.1049/ptee.1967.0306>
- Belrose JS (1970) Radio wave probing of the ionosphere by the partial reflection of radio waves (from heights below 100 km). *J Atmos Terr Phys* 32:567, [http://dx.doi.org/10.1016/0021-9169\(70\)90209-6](http://dx.doi.org/10.1016/0021-9169(70)90209-6)
- Bennett JA, Dyson PL (1993) On Pfister's theorem and its generalization. *J Atmos Terr Phys* 55:1307-10, [http://dx.doi.org/10.1016/0021-9169\(93\)90055-4](http://dx.doi.org/10.1016/0021-9169(93)90055-4)
- Bertoni FCP, Raulin J-P, Gavilán HR, Kaufmann P, Rodriguez R, Clilverd M, Cardenas JS, Fernandez G (2013) Lower ionosphere monitoring by the South America VLF network (SAVNET): C region occurrence and atmospheric temperature variability. *J Geophys Res Space Physics* 118:6686-93, <http://dx.doi.org/10.1002/jgra.50559>
- Bowles, K. L. (1964) Radiowave scattering in the ionosphere, in *Advances in Electronics and Electron Physics*, 19, ed. L. Marton, Academic Press; 55-176, [http://dx.doi.org/10.1016/S0065-2539\(08\)60845-8](http://dx.doi.org/10.1016/S0065-2539(08)60845-8)
- Breit G, Tuve MA (1925) A radio method of estimating the height of the conducting layer. *Nature* 116:357, <http://dx.doi.org/10.1038/116357a0>
- Breit G, Tuve MA (1926) A test of the existence of the conducting layer. *Phys Rev* 28:554, <http://dx.doi.org/10.1103/PhysRev.28.554>
- Brekke A, Holt O, Dickinson PHG, Friedrich M, Hansen T, Stauning P (1985) Development of D-region electron and ion densities under various auroral conditions during the Energy Budget Campaign (EBC). *J Atmos Terr Phys* 47:101, [http://dx.doi.org/10.1016/0021-9169\(85\)90127-8](http://dx.doi.org/10.1016/0021-9169(85)90127-8)
- Briggs BH (1980) Radar observations of atmospheric winds and turbulence: a comparison of techniques. *J Atmos Terr Phys* 42:823-33, [http://dx.doi.org/10.1016/0021-9169\(80\)90086-0](http://dx.doi.org/10.1016/0021-9169(80)90086-0)
- Briggs BH (1984) The analysis of spaced sensor records by correlation techniques, *Handbook for MAP*, 13, 166-186, SCOSTEP Secretariat. Univ. of Illinois, Urbana
- Briggs BH (1993) Observations of atmospheric dynamics using radar techniques. *Aust J Phys* 46(1):127-48, <http://dx.doi.org/10.1071/PH930127>
- Briggs BH (1994) The spaced-receiver technique. *J Atmos Terr Phys* 56:831-4, [http://dx.doi.org/10.1016/0021-9169\(94\)90140-6](http://dx.doi.org/10.1016/0021-9169(94)90140-6)
- Briggs BH (1995) On radar interferometric techniques in the situation of volume scatter. *Radio Sci* 30(1):109-14, <http://dx.doi.org/10.1029/94RS02415>
- Briggs BH, Holmes N (1973) Ionospheric observations using an ultrasonic image forming technique. *Nature Phys Sci* 243:111, <http://dx.doi.org/10.1038/physci243111a0>
- Briggs BH, Vincent RA (1992) Spaced-antenna analysis in the frequency domain. *Radio Sci* 27(2):117-29, <http://dx.doi.org/10.1029/91RS03051>
- Briggs BH, Elford WG, Felgate DG, Golley MG, Rossitter DE, Smith JW (1969) Buckland park aerial array. *Nature* 223:1321-5, <http://dx.doi.org/doi:10.1038/2231321a0>
- Burrage MD, Skinner WR, Gell DA, Hays DA, Marshall AR, Ortland DA, et al. Vincent (1996) Validation of mesosphere and lower thermosphere winds from the high resolution Doppler imager on UARS. *J Geophys Res* 101(D6):10365-92, <http://dx.doi.org/10.1029/95JD01700>
- Cervera MA, Reid IM (1995) Comparison of simultaneous wind measurements using collocated VHF meteor radar and MF spaced antenna radar systems. *Radio Sci* 30:1245-61, <http://dx.doi.org/10.1029/95RS00644>
- Champion KSW (1987) Middle atmosphere models and comparison with shuttle re-entry density data. *Adv Space Res* 7(10):77-82, [http://dx.doi.org/10.1016/0273-1177\(87\)90080-9](http://dx.doi.org/10.1016/0273-1177(87)90080-9)
- Chau JL (2000) A review of radar interferometric/imaging techniques used in MST radars, *Proc. 9th Workshop on Technical and Scientific Aspects of MST radar, SCOSTEP*. pp 25-34
- Chisham G, Freeman MP (2013) A reassessment of SuperDARN meteor echoes from the upper mesosphere and lower thermosphere. *J Atmos Solar Terr Physics* 102:207-21, <http://dx.doi.org/10.1016/j.jastp.2013.05.018>
- Cohn SA, Brown WOJ, Martin CL, Susedik MS, Maclean G, Parsons DB (2001) Clear air boundary layer spaced antenna wind measurement with the multiple antenna profiler (MAPR). *Ann Geophys* 19:845-54, <http://dx.doi.org/10.5194/angeo-19-845-2001>
- Czechowsky P, Schmidt G, Kopka H (1983) Medium frequency radar observations in the middle atmosphere. *J Atmos Terr Phys* 45:729-32, [http://dx.doi.org/10.1016/S0021-9169\(83\)80031-2](http://dx.doi.org/10.1016/S0021-9169(83)80031-2)
- Deeks DG (1966) D-region electron density distributions in middle latitudes deduced from the reflection of long radio waves. *Proc Roy Soc A* 291:413, <http://dx.doi.org/10.1098/rspa.1966.0103>



- Dieminger W (1952) Über die Ursache der excessiven absorption in der Ionosphären Wintertagen. *J Atmos Terr Phys* 2:340–9, [http://dx.doi.org/10.1016/0021-9169\(52\)90074-3](http://dx.doi.org/10.1016/0021-9169(52)90074-3)
- Dieminger W, Hofmann-Heyden AE (1952) Reflexionen von Kurzwellen aus Höhen unter 100 km. *Naturwissenschaften* 39:84–5, <http://dx.doi.org/10.1007/BF00631093>
- Dolman, B.K. and I.M. Reid (2014) Bias correction and overall performance of a VHF spaced antenna boundary layer profiler for operational weather forecasting. *J Atmos. Solar Terr Physics*. <http://dx.doi.org/10.1016/j.jastp.2014.02.009>
- Doviak RJ, Lataitis RJ, Holloway CL (1996) Cross correlation and cross spectra for spaced antenna wind profilers: 1. Theoretical analysis. *Radio Sci* 31:157–80, <http://dx.doi.org/10.1029/95RS02318>
- Elford, W.G (2001) Novel applications of MST radars in meteor studies. *J Atmos Solar Terr. Physics*, 63. [http://dx.doi.org/10.1016/S1364-6826\(00\)00145-0](http://dx.doi.org/10.1016/S1364-6826(00)00145-0)
- Elford WG, Elford MT (2001). The effective diffusion coefficient of meteor trails above 100 km. In: *Proceedings of the Meteoroids 2001 Conference*, Kiruna, Sweden. ESA Publications Division, ESA SP-495, Noordwijk, pp 357–9, ISBN 92-9092-805-0, 2001
- Ellyett WL (1947) Echoes at D-heights with special reference to the Pacific Islands. *Terr Magn Atmos Electr* 52(1):1–13, <http://dx.doi.org/10.1029/TE052i001p00001>
- Ellyett C, Watts JM (1959) Stratification in the lower ionosphere. *J Res NBS* 63D:117–34, <http://dx.doi.org/10.6028/jres.063D.016>
- Fan X, Weng LB, Zhang JB, Xie YQ (2014) Investigation of the mesospheric temperature over Fort Collins region. *Sci China Tech Sci* 57:1562–7, <http://dx.doi.org/10.1007/s11431-014-5593-2>
- Felgate DG (1970) On the point source effect in the measurement of ionospheric drifts. *J Atmos Terr Phys* 32:241–245, [http://dx.doi.org/10.1016/0021-9169\(70\)90196-0](http://dx.doi.org/10.1016/0021-9169(70)90196-0)
- Felgate DG, Golley MG (1971) Ionospheric irregularities and movements observed with a large aerial array. *J Atmos Terr Phys* 33:1353, [http://dx.doi.org/10.1016/0021-9169\(71\)90009-2](http://dx.doi.org/10.1016/0021-9169(71)90009-2)
- Flock WL, Balsley BB (1967) VHF radar returns from the D-region of the equatorial ionosphere. *J Geophys Res* 72:5537–41, <http://dx.doi.org/10.1029/JZ072i021p05537>
- Fraser GJ (1965) The measurement of atmospheric winds at altitudes of 64–120 km using ground-based radio equipment. *J Atmos Sci* 22:217–8, [http://dx.doi.org/10.1175/1520-0469\(1965\)022<0217:TMOAWA>2.0.CO;2](http://dx.doi.org/10.1175/1520-0469(1965)022<0217:TMOAWA>2.0.CO;2)
- Fraser GJ (2005) The antecedents and subsequent development of scientific radar in New Zealand. *J Atmos Solar Terr Physics* 67:1411–8, <http://dx.doi.org/10.1016/j.jastp.2005.07.010>
- Friedrich M, Torkar KM (1983) Collision frequencies in the high-latitude D-region. *J Atmos Terr Phys* 45(4):267, [http://dx.doi.org/10.1016/S0021-9169\(83\)80048-8](http://dx.doi.org/10.1016/S0021-9169(83)80048-8)
- Gardner FF, Pawsey JL (1953) Study of the ionospheric D-region using partial reflections. *J Atmos Terr Phys* 3(6):321–4, [http://dx.doi.org/10.1016/0021-9169\(53\)90084-1](http://dx.doi.org/10.1016/0021-9169(53)90084-1)
- Gnanalingham S, Weekes K (1952) Weak echoes from the ionosphere with radiowaves of frequency 1.42 MHz. *Nature* 170:113–4, <http://dx.doi.org/10.1038/170113b0>
- Golley MG, Rossiter DE (1970) Some tests of methods of analysis of ionospheric drift records using an array of 89 aerials. *J Atmos Terr Phys* 32:1215–33, [http://dx.doi.org/10.1016/0021-9169\(70\)90053-X](http://dx.doi.org/10.1016/0021-9169(70)90053-X)
- Greenhow JS, Hall JE (1960) The importance of initial trail radius on the apparent height and number distributions of meteor echoes. *MNRAS* 121:183–96, <http://dx.doi.org/10.1093/mnras/121.2.183>
- Gregory JB (1956) Ionospheric reflections from heights below the E-region. *Aust J Phys* 9:324, <http://dx.doi.org/10.1071/PH560324>
- Gregory JB (1961) Radio wave reflections from the mesosphere: 1. Heights of occurrence. *J Geophys Res* 66(2):429–45, <http://dx.doi.org/10.1029/JZ066i002p00429>
- Gregory JB, Meek CE, Manson AH, Stephenson DG (1979) Developments in the radiowave drifts technique for measurement of high-altitude winds. *J Appl Meteorol* 18:682–91, [http://dx.doi.org/10.1175/1520-0450\(1979\)018<0682:DITRDT>2.0.CO;2](http://dx.doi.org/10.1175/1520-0450(1979)018<0682:DITRDT>2.0.CO;2)
- Hall C (2000) The Ramfjordmoen MF radar (69N, 19E): application development 1990–2000. *J Atmos Terr Phys* 63:171–9, [http://dx.doi.org/10.1016/S1364-6826\(00\)00144-9](http://dx.doi.org/10.1016/S1364-6826(00)00144-9)
- Hall CM, Manson AH, Meek CE (1998) Seasonal variation of the turbopause: one year of turbulence investigation at 69°N by the joint University of Tromsø/University of Saskatchewan MF radar. *J Geophys Res* 103(D22):28769–73, <http://dx.doi.org/10.1029/1998JD200002>
- Hall CM, Manson AH, Meek CE, Nozawa S (2006) Isolated lower mesospheric echoes seen by medium frequency radar at 70° N, 19° E. *Atmos Chem Phys* 6:5307–14, <http://dx.doi.org/10.5194/acp-6-5307-2006>
- Hauchecorne A, Chanin ML, Wilson R (1987) Mesospheric temperature inversion and gravity wave breaking. *Geophys Res Lett* 14:933–6, <http://dx.doi.org/10.1029/GL014i009p00933>
- Hedin J, Gumbel J, Khaplanov M, Witt G, Stegman J (2008) Optical studies of noctilucent clouds in the extreme ultraviolet. *Ann Geophys* 26:1109–19, <http://dx.doi.org/10.5194/angeo-26-1109-2008>
- Hines CO, Rhagava Rao R (1968) Validity of three station methods of determining ionospheric motions. *J Atmos Terr Phys* 30:979–93, [http://dx.doi.org/10.1016/S0021-9169\(68\)80048-0](http://dx.doi.org/10.1016/S0021-9169(68)80048-0)
- Hines CO, Adams GW, Brosnahan JW, Djuth FT, Sulzer MP, Tepley CA, Van Baelen JS (1993) Multi-instrument observations of mesospheric motions over Arecibo: comparisons and interpretations. *J Atmos Sol Terr Phys* 55(3):241–87, [http://dx.doi.org/10.1016/0021-9169\(93\)90069-B](http://dx.doi.org/10.1016/0021-9169(93)90069-B)
- Hocking WK (1981) Investigation of the movement and structure of D-region ionospheric irregularities. PhD Thesis, Adelaide University, Australia
- Hocking WK (1983) On the extraction of atmospheric turbulence parameters from radar backscatter Doppler spectra—I. Theory. *J Atmos Terr Phys* 45:89–102, [http://dx.doi.org/10.1016/S0021-9169\(83\)80013-0](http://dx.doi.org/10.1016/S0021-9169(83)80013-0)
- Hocking WK (1997) Strengths and limitations of MST radar measurements of middle-atmosphere winds. *Ann Geophys* 15:1111–22, <http://dx.doi.org/10.1007/s00585-997-1111-1>
- Hocking WK (2005) A new approach to momentum flux determinations using SKIYMET meteor radars. *ANGEOS* 23(7):2433–9, <http://dx.doi.org/10.5194/angeo-23-2433-2005>
- Hocking WK (2011) A review of mesosphere–stratosphere–troposphere (MST) radar developments and studies, circa 1997–2008. *J Atmos Sol Terr Phys* 73:848–82, <http://dx.doi.org/10.1016/j.jastp.2010.12.009>
- Hocking WK, Thayapaxan T (1997) Simultaneous and co-located observations of winds and tides by MF and meteor radars over London, Canada (43N, 81W) during 1994–1996. *Radio Sci* 32:835–67, <http://dx.doi.org/10.1029/1999GL003618>
- Hocking WK, May PT, Röttger J (1989) Interpretation, reliability and accuracies of parameters deduced by the spaced antenna method in middle atmosphere applications. *PureAppl Geophys* 130:571–604, <http://dx.doi.org/10.1007/BF00874475>
- Hocking WK, Fuller B, Vandepuer B (2001) Real-time determination of meteor-related parameters utilizing modern digital technology. *J Atmos Sol Terr Phys* 63:155–69, [http://dx.doi.org/10.1016/S1364-6826\(00\)00138-3](http://dx.doi.org/10.1016/S1364-6826(00)00138-3)
- Hoffmann P, Singer W, Kreuer D, Schminder R, Kürschner D (1990) Partial reflection drift measurements in the lower ionosphere over Juliusruh during winter and spring 1989 and comparison with other wind observations. *Zeit Meteorol* 40:405–12
- Hoffmann P, Rapp M, Singer W, Keuer D (2011) Trends of mesospheric gravity waves at northern middle latitudes during summer. *J Geophys Res* 116:D00P08, <http://dx.doi.org/10.1029/2011JD015717>
- Holdsworth DA (1999) Influence of instrumental effects upon the full correlation analysis. *Radio Sci* 34(3):643–55. doi:10.1029/1999RS900001
- Holdsworth DA, Reid IM (1995a) A simple model of atmospheric radar backscatter: description and application to the full correlation analysis of spaced antenna data. *Radio Sci* 30(4):1263–80, <http://dx.doi.org/10.1029/95RS00645>
- Holdsworth DA, Reid IM (1995b) Spaced antenna analysis of atmospheric radar backscatter model data. *Radio Sci* 30(5):1417–33, <http://dx.doi.org/10.1029/95RS01888>
- Holdsworth DA, Reid IM (1997) An investigation of biases in the full correlation analysis technique. *Adv Space Res* 20(6):1281–4, [http://dx.doi.org/10.1016/S0273-1177\(97\)00784-9](http://dx.doi.org/10.1016/S0273-1177(97)00784-9)
- Holdsworth DA, Reid IM (2004a) The Buckland Park MF radar: routine observation scheme and velocity comparisons. *Ann Geophys* 22:3815–28, <http://dx.doi.org/10.5194/angeo-22-3815-2004>
- Holdsworth DA, Reid IM (2004b) Comparisons of full correlation analysis (FCA) and imaging Doppler interferometry (IDI) winds using the Buckland Park MF radar. *Ann Geophys* 22(11):3829–42, <http://dx.doi.org/10.5194/angeo-22-3829-2004>
- Holdsworth DA, Vincent RA, Reid IM (2001) Mesospheric turbulent velocity estimation using the Buckland Park MF radar. *Ann Geophys* 19(8):1007–17, <http://dx.doi.org/10.5194/angeo-19-1007-2001>
- Holdsworth DA, Vuthaluru R, Reid IM, Vincent RA (2002) Differential absorption measurements of mesospheric and lower thermospheric electron densities using the Buckland Park MF radar. *J Atmos Sol Terr Phys* 64:2029–42, [http://dx.doi.org/10.1016/S1364-6826\(02\)00232-8](http://dx.doi.org/10.1016/S1364-6826(02)00232-8)

- Holdsworth DA, Reid IM, Cervera MA (2004a) The Buckland Park all-sky interferometric meteor radar—description and first results. *Radio Sci* 39:RS5009, <http://dx.doi.org/10.1029/2003RS003014>
- Holdsworth DA, Tsutsumi M, Reid IM, Nakamura T, Tsuda T (2004b) Interferometric meteor phase calibration using meteor echoes, *Radio Sci*. RS5012, <http://dx.doi.org/10.1029/2003RS003026>
- Holdsworth DA, Morris RJ, Murphy DJ, Reid IM, Burns GB, French WJR (2006) Antarctic mesospheric temperature estimation using the Davis VHF radar. *J Geophys Res* 111:D05108, <http://dx.doi.org/10.1029/2005JD006589>
- Holdsworth DA, Elford WG, Vincent RA, Reid IM, Murphy Damian J, Singer W (2007) All-sky interferometric meteor radar meteoroid speed estimation using the Fresnel transform. *ANGEOS* 25(2):385–98, <http://dx.doi.org/10.5194/angeo-25-385-2007>
- Holloway CL, Doviak RJ, Cohn SA, Lataitis RJ, Van Baelen JS (1997) Cross correlations and cross spectra for spaced antenna wind profilers: 2. Algorithms to estimate wind and turbulence. *Radio Sci* 32:967–82, <http://dx.doi.org/10.1029/96RS03885>
- Holmes NE (1975) An ultrasonic image-forming system for use with multi-element antenna arrays. *Proc Inst Radio Electron Eng Aust* 36(10):321–8
- Jacobi C (2014) Long-term trends and decadal variability of upper mesosphere/lower thermosphere gravity waves at midlatitudes. *J Atmos Solar Terr Phys* 118:90–5, <http://dx.doi.org/10.1016/j.jastp.2013.05.009>
- Jones J, Jones W (2006) Meteor radiant activity mapping using single-station radar observations. *MNRAS* 367:1050–6, <http://dx.doi.org/10.1111/j.1365-2966.2006.10025.x>
- Jones GOL, Charles K, Jarvis MJ (1997) First mesospheric observations using an imaging Doppler interferometer adaptation of the dynasonde at Halley, Antarctica. *Radio Sci* 32(6):2109–22, <http://dx.doi.org/10.1029/97RS01825>
- Jones GOL, Berkey FT, Fish CS, Hocking WK, Taylor MJ (2003) Validation of imaging Doppler interferometer winds using meteor radar. *Geophys Res Lett* 30(14):1743, <http://dx.doi.org/10.1029/2003GL017645>
- Jones GOL, Clilverd MA, Espy PJ, Chew S, Fritts DC, Riggan DM (2004) An alternative explanation of PMSE-like scatter in MF radar data. *Ann Geophys* 22:2715–22, <http://dx.doi.org/10.5194/angeo-22-2715-2004>
- Jursa, AS (1985) Handbook of geophysics and the space environment, Hanscom Air Force Geophysics Laboratory. [http://www.cnofs.org/Handbook\\_of\\_Geophysics\\_1985/Handbook.pdf](http://www.cnofs.org/Handbook_of_Geophysics_1985/Handbook.pdf)
- Kawamura S, M Tsutsumi, and Y Murayama (2007) Wind estimations with meteor observations by MF radars at Poker Flat, Alaska and Wakkanai, Japan. *J National Institute of Information and Communications Technology*. 54, Nos.1/2
- Khattatov BV, Geller MA, Yudin VA, Hays PB, Skinner WR, Burrage MD, Franke SJ, Fritts DC, Isler JR, Manson AH, Meek CE, McMurray R, Singer W, Hoffmann P, Vincent RA (1996) Dynamics of the mesosphere and lower thermosphere as seen by MF radars and by the high-resolution Doppler imager/JAARS. *J Geophys Res* 101(D6):10393–404, <http://dx.doi.org/10.1029/95JD01704>
- Kleinknecht NH, Espy PJ, Hibbins RE (2014) The climatology of zonal wave numbers 1 and 2 planetary wave structure in the MLT using a chain of Northern Hemisphere SuperDARN radars. *J Geophys Res Atmos* 119:1292–307, <http://dx.doi.org/10.1002/2013JD019850>
- Krautkrämer J (1950) Windmessungen in der Ionosphäre. *Arch elektr Übertragung* 4:133–41
- Kudeki E, Woodman RF (1990) A poststatistics steering technique for MST radar applications. *Radio Sci* 25(4):591–4, <http://dx.doi.org/10.1029/RS025i004p00591>
- Kudeki E, Rastogi PK, Sürücü F (1993) Systematic errors in radar wind estimation: implications for comparative measurements. *Radio Sci* 28(2):169–79, <http://dx.doi.org/10.1029/92RS01931>
- Lataitis RJ, Clifford SF, Holloway CL (1995) An alternate method for inferring winds from spaced-antenna radar measurements. *Radio Sci* 30:463–74, <http://dx.doi.org/10.1029/94RS02414>
- Lesicar D, Hocking WK, Vincent RA (1994) Comparative studies of scatterers observed by MF radars in the southern hemisphere mesosphere. *J Atmos Terr Phys* 56:581–91, [http://dx.doi.org/10.1016/0021-9169\(94\)90099-X](http://dx.doi.org/10.1016/0021-9169(94)90099-X)
- Li G, Ning B, Hu L, Chu Y-H, Reid IM, Dolman B (2012) A comparison of lower thermospheric winds derived from range spread and specular meteor trail echoes. *J Geophys Res* 117:A03310, <http://dx.doi.org/10.1029/2011JA016847>
- Lingard DM (1996a) A deconvolution technique for measuring D-region radio wave backscatter. *J Atmos Sol Terr Phys* 58(11):1201–9, [http://dx.doi.org/10.1016/0021-9169\(95\)00150-6](http://dx.doi.org/10.1016/0021-9169(95)00150-6)
- Lingard DM (1996b) Comparison of a deconvolution technique for measuring mesospheric winds with the spaced antenna technique. *J Atmos Sol Terr Phys* 58(11):1211–8, [http://dx.doi.org/10.1016/0021-9169\(95\)00151-4](http://dx.doi.org/10.1016/0021-9169(95)00151-4)
- Luce H, Crochet M, Dalaudier F (2001) Temperature sheets and aspect sensitive radar echoes. *Ann Geophys* 19:899–920, <http://dx.doi.org/10.5194/angeo-19-899-2001>
- MacKinnon AD, Vincent RA, Reid IM (2002) Boundary layer radar measurements during DAWEX, in International Symposium on Equatorial Processes Including Coupling (EPIC). Int. Union of Radio Sci, Kyoto, Japan, pp 478–80, 18–22 March
- Manson AH, Meek CE (1984) Partial reflection D-region electron densities, Handbook for MAP, 13, ed. R.A. Vincent, SCOSTEP Secretariat, 113–123
- Mayo R (2015) Pulse Coding, Characteristics and Implementation on ATRAD Radars, ATRAD Technical Report, Document No: 15-70052. ATRAD Pty Ltd, Adelaide, Australia
- McIntosh DL (2010) Comparisons of VHF meteor radar observations in the middle atmosphere with multiple independent remote sensing techniques, PhD thesis, University of Adelaide. <http://hdl.handle.net/2440/60068>
- McKinley DWR (1951) Variation of meteor echo rates with radar system parameters. *Can J Phys* 29:403–26
- Meek CE (1980) An efficient method for analysing ionospheric drifts data. *J Atmos Terr Phys* 42:835–9, [http://dx.doi.org/10.1016/0021-9169\(80\)90087-2](http://dx.doi.org/10.1016/0021-9169(80)90087-2)
- Meek CE, Manson AH (1987) Mesospheric motions observed by simultaneous medium-frequency interferometer and spaced antenna experiments. *J Geophys Res* 92(D5):5627–39, <http://dx.doi.org/10.1029/JD092iD05p05627>
- Meek CE, Manson AH (2001) MF radar spaced antenna experiment: wind variance vs. record length. *J Atmos Sol Terr Phys* 63:181–91, [http://dx.doi.org/10.1016/S1364-6826\(00\)00148-6](http://dx.doi.org/10.1016/S1364-6826(00)00148-6)
- Meek CE, Reid IM, Manson AH (1986a) Comparison of medium frequency pulsed radar interferometer and correlation analysis winds: 1, Handbook for MAP, 20. SCOSTEP Secretariat, University of Illinois, Urbana, USA, pp 293–8
- Meek CE, Reid IM, Manson AH (1986b) Comparison of medium frequency pulsed radar interferometer and correlation analysis winds: 2, Handbook for MAP, 20. SCOSTEP Secretariat, University of Illinois, Urbana, USA, pp 299–302
- Mitra SN (1949) A radio method of measuring winds in the ionosphere. *Proc Instn Elect Engrs* 96:441–6, <http://dx.doi.org/10.1049/pi-3.1949.0094>
- Morris RJ, Murphy DJ, Vincent RA, Holdsworth DA, Klekociuk AR, Reid IM (2006) Characteristics of the wind, temperature and PMSE field above Davis Antarctica. *J Atmos Solar Terr Physics* 68:418–35, <http://dx.doi.org/10.1016/j.jastp.2005.04.011>
- Murphy DJ, Vincent RA (1993) Estimates of momentum flux in the mesosphere and lower thermosphere over Adelaide, Australia, from March 1985 to February 1986. *J Geophys Res* 98(D10):18617–38, <http://dx.doi.org/10.1029/93JD01861>
- Muschinski A, Sullivan PP (2013) Using large-eddy simulation to investigate intermittency fluxes of clear-air radar reflectivity in the atmospheric boundary layer, 2013 IEEE Antennas and Propagation Society International Symposium (APSURS). 2321 – 2322. <http://dx.doi.org/10.1109/APS.2013.6711819>
- Namboothiri SP, Manson AH, Meek CE (1993) E region real heights and their implications for MF radar-derived wind and tidal climatologies. *Radio Sci* 28(2):187–202, <http://dx.doi.org/10.1029/92RS02458>
- Namboothiri SP, Manson AH, Meek CE (1994) Extension of MF radar tidal measurements to E-region heights (95–125 km): Saskatoon (52°N, 107°W), Canada. *Ann Geophys* 12:333–41, <http://dx.doi.org/10.1007/s00585-994-0333-8>
- Nicolet M, Aikin AC (1960) The formation of the D region of the ionosphere. *J Geophys Res* 65:1469–83, <http://dx.doi.org/10.1029/JZ065i005p01469>
- Offermann D, Gerndt R, Küchler R, Baker K, Pendleton WR, Meyer W, von Zahn U, Philbrick CR, Schmidlin FJ (1987) Mean state and long term variations of temperature in the winter middle atmosphere above northern Scandinavia. *J Atmos Terr Phys* 49:655–74, [http://dx.doi.org/10.1016/0021-9169\(87\)90011-0](http://dx.doi.org/10.1016/0021-9169(87)90011-0)
- Palo SE, Hagan ME, Meek CE, Vincent RA, Burrage MD, McLandress CS et al (1997) An intercomparison between the GSWM, UARS, and ground based radar observations: a case-study in January 1993, *Ann Geophysicae* 15, 1123–1141, <http://dx.doi.org/10.1007/s00585-997-1123-x>
- Pancheva D, Mitchell NJ, Hagan ME, Manson AH, Meek CE, Yi L, Ch J, Kürschner D, Clark RR, Hocking WK, MacDougall J, Jones GOL, Vincent RA, Reid IM, Singer W, Igarashi K, Fraser G, Nakamura T, Tsuda T, Yu P, Merzlyakov E, Fahrutdinova AN, Stepanov AM, Poole LMG, Malinga SB, Kashcheyev BL, Oleynikov AN, Riggan DM (2002) Global-scale tidal structure in the mesosphere and lower thermosphere during the PSMOS campaign of June–August 1999 and comparisons with the global-scale wave model. *J Atmos Solar Terr Physics* 64:1011–35, [http://dx.doi.org/10.1016/S1364-6826\(02\)00054-8](http://dx.doi.org/10.1016/S1364-6826(02)00054-8)
- Pavlov AV (2014) Photochemistry of ions at D-region altitudes of the ionosphere: a review. *Surv Geophys* 35:259–334, <http://dx.doi.org/10.1007/s10712-013-9253-z>
- Pawsey JL (1935) Further investigations of the amplitude variations of downcoming wireless waves. *Proc Camb Phil Soc* 31:125, <http://dx.doi.org/10.1017/S0305004100013025>

- Pfister W (1971) The wave-like nature of inhomogeneities in the E-region. *J Atmos Terr Phys* 33:999–1025, [http://dx.doi.org/10.1016/0021-9169\(71\)90123-1](http://dx.doi.org/10.1016/0021-9169(71)90123-1)
- Phillips GJ, Spencer M (1955) The effects of anisometric amplitude patterns in the measurement of ionospheric drifts. *Proc Phys Soc, B* 68:481, <http://dx.doi.org/10.1088/0370-1301/68/8/301>
- Pineo VC (1956) Oblique-incidence measurements of the heights at which ionospheric scattering of VHF radio waves occurs. *J Geophys Res* 61:165–9, <http://dx.doi.org/10.1029/JZ061i002p00165>
- Placke M (2013) Gravity waves and momentum fluxes in the mesosphere and lower thermosphere region, PhD Thesis, University of Rostock. 51 pp
- Placke MP, Hoffmann R, Latteck M, Rapp (2015) Gravity wave momentum fluxes from MF and meteor radar measurements in the polar MLT region, *J Geophys Res Space Physics*. <http://dx.doi.org/10.1002/2014JA020460>
- Priese J, Singer W (1984) Measurements of partial reflections at 3.18 MHz using the CW-radar technique. *Handbook for Middle Atmosphere Program 10:39*
- Ratcliffe JA (1956) Some aspects of diffraction theory and their application to the ionosphere. *Rep Prog Phys* 19:188, <http://dx.doi.org/10.1088/0034-4885/19/1/306>
- Ratcliffe JA, Pawsey JL (1933) A study of the intensity variations of downcoming wireless waves. *Math Proc Camb Philos Soc* 29:301–18, <http://dx.doi.org/10.1017/S0305004100011117>
- Reber CA, Trevathan CE, McNeal RJ, Luther MR (1993) The Upper Atmosphere Research Satellite (UARS) mission. *Geophys Res* 98:10,643–10,647, <http://dx.doi.org/10.1029/92JD02828>
- Reid IM (1987) Some aspects of Doppler radar measurements of the mean and fluctuating components of the wind field in the upper middle atmosphere. *J Atmos Terr Phys* 49:467–84, [http://dx.doi.org/10.1016/0021-9169\(87\)90041-9](http://dx.doi.org/10.1016/0021-9169(87)90041-9)
- Reid IM (1988) MF Doppler and spaced antenna measurements of upper middle atmosphere winds. *J Atmos Terr Phys* 50:117–34, [http://dx.doi.org/10.1016/0021-9169\(88\)90049-9](http://dx.doi.org/10.1016/0021-9169(88)90049-9)
- Reid IM (1990) Radar observations of stratified layers in the mesosphere and lower thermosphere (50–100 km). *Adv Space Res* 10(10):7–19, [http://dx.doi.org/10.1016/0273-1177\(90\)90002-H](http://dx.doi.org/10.1016/0273-1177(90)90002-H)
- Reid IM (1996) On the measurement of gravity waves, tides and mean winds in the low and middle latitude mesosphere and thermosphere with MF radar. *Adv Space Res* 18:131–40, [http://dx.doi.org/10.1016/0273-1177\(95\)00852-6](http://dx.doi.org/10.1016/0273-1177(95)00852-6)
- Reid IM, Vincent RA (1987) Measurements of mesospheric gravity wave momentum fluxes and mean flow accelerations at Adelaide, Australia. *J Atmos Terr Phys* 49:443–60, [http://dx.doi.org/10.1016/0021-9169\(87\)90039-0](http://dx.doi.org/10.1016/0021-9169(87)90039-0)
- Reid IM, Vandeppeer BGW, Dillon SD, Fuller BG (1995) The new Adelaide MF Doppler radar. *Radio Sci* 30:1177–89, <http://dx.doi.org/10.1029/95RS00731>
- Reid IM, Holdsworth DA, Kovalam S, Vincent RA, Stickland J (2005) Mount Gambier (38°S, 141°E) prototype VHF wind profiler. *Radio Sci* 40:RS5007, <http://dx.doi.org/10.1029/2004RS003055>
- Reinisch B, Scali JL, Haines DM (1998) Ionospheric drift measurements with ionosondes. *Ann Geophys* 41:695–702
- Rietveld MT, Wright JW, Zaboltn N, Pitteway MLV (2008) The Tromsø dynasonde. *Polar Science* 2(1):55–71, <http://dx.doi.org/10.1016/j.polar.2008.02.001>
- Rong PP, Yue J, Russell III JM, Lumpe JD, Gong J, Wu DL, Randall CE (2015) Horizontal winds derived from AIM CIPS polar mesospheric cloud images, *J Geophys Res Atmos*. 120, <http://dx.doi.org/10.1002/2014JD022813>
- Røyrvik O (1983) Spaced antenna drift at Jicamarca, mesospheric measurements. *Radio Sci* 18(3):461–76, <http://dx.doi.org/10.1029/RS018i003p00461>
- Schmidlin FJ (1976) Temperature inversions near 75 km. *Geophys Res Lett* 3:173–6, <http://dx.doi.org/10.1029/GL003i003p00173>
- Schminder R, Kürschner D (1994) Permanent monitoring of the upper mesosphere and lower thermosphere wind fields (prevailing and semidiurnal tidal components) obtained from LF D1 measurements in 1991 at the Collm Geophysical Observatory. *J Atmos Terr Phys* 56(10):1263–9, [http://dx.doi.org/10.1016/0021-9169\(94\)90064-7](http://dx.doi.org/10.1016/0021-9169(94)90064-7)
- Singer W, Priese J, Hoffmann P (1988) Experimental technique of lower ionosphere electron density measurements by means of partial reflections. *Adv Space Res* 8(4):49, [http://dx.doi.org/10.1016/0273-1177\(88\)90203-7](http://dx.doi.org/10.1016/0273-1177(88)90203-7)
- Singer W, Latteck R, Holdsworth DA, Kristiansen T (2003). A new narrow beam MF radar at 3 MHz for studies of the high-latitude middle atmosphere: system description and first results, *Proc. of the 10th Workshop on Tech., Sci. Aspects of MST Radar in Piura, Peru*, [http://jro.igpp.gob.pe/mst10/CD/ExtAbs/Session5/IS\\_015.pdf](http://jro.igpp.gob.pe/mst10/CD/ExtAbs/Session5/IS_015.pdf)
- Singer W, Latteck R, Holdsworth DA (2008) A new narrow beam Doppler radar at 3 MHz for studies of the high-latitude middle atmosphere. *Adv Space Res* 41(9):1488–94, <http://dx.doi.org/10.1016/j.asr.2007.10.006>
- Singer W, Latteck R, Friedrich M, Wakabayashi M, Rapp M (2011) Seasonal and solar activity variability of D-region electron density at 69°N. *J Atmos Sol Terr Phys* 73:925–35, <http://dx.doi.org/10.1016/j.jastp.2010.09.012>
- Spargo AJ, Reid IM, MacKinnon AD (2015) Gravity wave momentum transport measurements in the mesosphere lower thermosphere/ionosphere region using partial reflection and meteor radar, paper IUGG-5011, M14 Middle Atmosphere Science, 26<sup>th</sup> IUGG General Assembly, Prague
- Sprenger K, Schminder R (1969) On some relationships between correlation analysis and similar-fade analysis results of drift measurements in the lower ionosphere. *J Atmos Terr Phys* 31:1085–98, [http://dx.doi.org/10.1016/0021-9169\(69\)90107-X](http://dx.doi.org/10.1016/0021-9169(69)90107-X)
- Steel DI, Elford WG (1991) The height distribution of radio meteors: comparison of observations at different frequencies on the basis of standard echo theory. *J Atmos Terr Phys* 53:409–17, [http://dx.doi.org/10.1016/0021-9169\(91\)90035-6](http://dx.doi.org/10.1016/0021-9169(91)90035-6)
- Stubbs TJ (1973) The measurement of winds in the D-region of the ionosphere by the use of partially reflected radio waves. *J Atmos Terr Phys* 35:909–19, [http://dx.doi.org/10.1016/0021-9169\(73\)90072-X](http://dx.doi.org/10.1016/0021-9169(73)90072-X)
- Suruca F, Franke SJ, Kudeki E (1995) On the influence of specular reflections in MF radar wind measurements. *Radio Sci* 30:1229–44, <http://dx.doi.org/10.1029/94RS03166>
- Thayaparan T, Hocking WK (2002) A long-term comparison of winds and tides measured at London, Canada (43°N, 81°W) by co-located MF and meteor radars during 1994–1999. *J Atmos Sol Terr Phys* 64:931–46, [http://dx.doi.org/10.1016/S1364-6826\(02\)00048-2](http://dx.doi.org/10.1016/S1364-6826(02)00048-2)
- Thomson NR, Ciliverd MA, McRae WM (2007) Nighttime ionospheric D region parameters from VLF phase and amplitude. *J Geophys Res* 112:A07304, <http://dx.doi.org/10.1029/2007JA012271>
- Thorsen D, Franke SJ, Kudeki E (1997) A new approach to MF radar interferometry for estimating mean winds and momentum flux. *Radio Sci* 32(2):707–26, <http://dx.doi.org/10.1029/96RS03422>
- Thrane EV, Piggott WR (1966) The collision frequency in the D- and E-regions of the ionosphere. *J Atmos Terr Phys* 28:721, [http://dx.doi.org/10.1016/0021-9169\(66\)90056-0](http://dx.doi.org/10.1016/0021-9169(66)90056-0)
- Titheridge JE (1962) The stratification of the lower ionosphere. *J Atmos Terr Phys* 24:283–96, [http://dx.doi.org/10.1016/0021-9169\(62\)90098-3](http://dx.doi.org/10.1016/0021-9169(62)90098-3)
- Tsuda T, Gordon WE, Saito H (1997) Azimuth-angle variations of specular reflection echoes in the lower atmosphere observed with the MU radar. *J Atmos Terr Phys* 59:777–84, [http://dx.doi.org/10.1016/S1364-6826\(96\)00058-2](http://dx.doi.org/10.1016/S1364-6826(96)00058-2)
- Tsutsumi M, Aso T (2005) MF radar observations of meteors and meteor-derived winds at Syowa (69S, 39E), Antarctica: a comparison with simultaneous spaced antenna winds. *J Geophys Res* 110:D24111, <http://dx.doi.org/10.1029/2005JD005849>
- Tsutsumi M, Holdsworth D, Nakamura T, Reid I (1999) Meteor observations with an MF radar. *Earth Planets Space* 51:691–9, <http://dx.doi.org/10.1186/BF03353227>
- Turek RS, Miller KL, Roper RG, Brosnahan JW (1995) Mesospheric wind studies during AIDA Act '89: morphology and comparison of various techniques. *J Atmos Terr Phys* 57:1321–43, [http://dx.doi.org/10.1016/0021-9169\(94\)00118-8](http://dx.doi.org/10.1016/0021-9169(94)00118-8)
- Valentic TA, Avery JP, Avery SK, Cervera MA, Elford WG, Vincent RA, Reid IM (1996) A comparison of meteor radar systems at Buckland Park. *Radio Sci* 31(6):1313–29, <http://dx.doi.org/10.1029/96RS02028>
- Vandeppeer BGW, Hocking WK (1993) A comparison of Doppler and spaced antenna techniques for the measurement of turbulent energy dissipation rates. *Geophys Res Lett* 20(1):17–20, <http://dx.doi.org/10.1029/92GL01116>
- Vandeppeer BGW, Reid IM (1995a) On the spaced antenna and imaging Doppler interferometer. *Radio Sci* 30:885–901, <http://dx.doi.org/10.1029/95RS00994>
- Vandeppeer BGW, Reid IM (1995b) Some preliminary results with the new Adelaide MF radar. *Radio Sci* 30:1191–203, <http://dx.doi.org/10.1029/95RS00732>
- Venkatesh V, Frasier SJ (2013) Simulation of spaced antenna wind retrieval performance on an X-band active phased array weather radar. *J Atmos Ocean Technol* 30:1447–59, <http://dx.doi.org/10.1175/jtech-d-11-00203.1>
- Vincent RA, Reid IM (1983) HF Doppler measurements of mesospheric gravity wave momentum fluxes. *J Atmos Sci* 40:1321–33, [http://dx.doi.org/10.1175/1520-0469\(1983\)040<1321:HDMOMG>2.0.CO;2](http://dx.doi.org/10.1175/1520-0469(1983)040<1321:HDMOMG>2.0.CO;2)
- von Biel HA (1977) The phase switched correlation polarimeter—a new approach to the partial reflection experiment. *J Atmos Terr Phys* 39:769, [http://dx.doi.org/10.1016/0021-9169\(77\)90138-6](http://dx.doi.org/10.1016/0021-9169(77)90138-6)
- Vuthaluru R, Vincent RA, Holdsworth DA, Reid IM (2002) Collision frequencies in the mid-latitude D-region. *J Atmos Sol Terr Phys* 64:2043–54, [http://dx.doi.org/10.1016/S1364-6826\(02\)00220-1](http://dx.doi.org/10.1016/S1364-6826(02)00220-1)

- Watson-Watt RA, Wilkins AF, Bowen EG (1937) The return of radio waves from the middle atmosphere, 1. *Proc Roy Soc A* 161:181–96, <http://dx.doi.org/10.1098/rspa.1937.0140>
- Weber BL, Wuertz DB (1991), Quality control algorithm for profiler measurements of winds and temperatures. NOAA Tech. Memo. ERL WPL-212, 32 pp. [NTIS PB92124080XSP]
- Whitehead JD, From WR, Jones KL, Monro PE (1983) Measurement of movements in the ionosphere using radio reflections. *J Atmos Terr Phys* 45:345–51, [http://dx.doi.org/10.1016/S0021-9169\(83\)80039-7](http://dx.doi.org/10.1016/S0021-9169(83)80039-7)
- Younger JP, Reid IM, Vincent RA (2013) Mutual coupling of antennas in a meteor radar interferometer. *Radio Sci* 48:118–21, <http://dx.doi.org/10.1002/rds.20026>
- Younger JP, Lee CS, Reid IM, Vincent RA, Kim YH, Murphy DJ (2014) The effects of deionization processes on meteor radar diffusion coefficients below 90 km. *J Geophys Res Atmos* 119:10,027–10,043, <http://dx.doi.org/10.1002/2014JD021787>
- Younger JP, Reid IM, Vincent RA, Murphy DJ (2015) A method for estimating the height of a mesospheric density level using meteor radar. *Geophys. Res. Lett.*, 42, <http://dx.doi.org/10.1002/2015GL065066>
- Yu T-Y, Palmer RD (2001) Atmospheric radar imaging using multiple-receiver and multiple-frequency techniques. *Radio Sci* 36:1493–503, <http://dx.doi.org/10.1029/2000RS002622>
- Zhang G, Doviak RJ (2007) Spaced-antenna interferometry to measure crossbeam wind, shear, and turbulence: theory and formulation. *J Atmos Ocean Technol* 24:791, <http://dx.doi.org/10.1175/JTECH2004.1>

**Submit your manuscript to a SpringerOpen<sup>®</sup> journal and benefit from:**

- Convenient online submission
- Rigorous peer review
- Immediate publication on acceptance
- Open access: articles freely available online
- High visibility within the field
- Retaining the copyright to your article

---

Submit your next manuscript at ► [springeropen.com](http://springeropen.com)

---